inhibition mechanism to decrease NMDAR activity (through reduction in D-serine synthesis) and prevent neurotoxicity at neighboring synapses. Notably, NMDAR-mediated translocation to the membrane is irreversible, even after blockade with NMDAR antagonists (Balan et al. 2009). The data indicate that NMDAR-mediated translocation is a last resort mechanism used by cells that are already committed to die. NMDAR-dependent inactivation of SR may protect neighboring cells by preventing further D-serine production and limiting the spread of excitotoxicity.

Another mechanism by which NMDAR activation controls SR activity involves NOS activation and SR nitrosylation at Cys113 (Mustafa et al. 2007). This leads to a decrease in SR activity via displacement of ATP binding (Mustafa et al. 2007). Thus, in addition to promoting SR translocation to the membrane (Balan et al. 2009), NMDAR activation inhibits SR activity via reversible *S*-nitrosylation. Diffusion of NO to non-neuronal cells will inactivate glial SR. On the other hand, NMDA-mediated SR translocation is NO independent, indicating that different cell types use different regulatory mechanisms involving different mediators.

Phosphorylation of mouse SR at Thr71 stimulates the rate of D-serine synthesis by increasing the turnover of the enzyme (Foltyn et al. 2010). Metabolic labeling indicates that this site comprises at least 80 % of the total SR phosphoprotein. Phosphorylation of SR at Thr71 was confirmed in vivo by phosphoproteome analysis of mouse brain (Wisniewski et al. 2010; Huttlin et al. 2010). The specific kinase has not been identified, though it likely belongs to the class of proline-directed kinases. This phosphorylation site, however, is not conserved in the human SR, indicating that it may mediate rodent-specific regulation/behavior.

SR inhibitors

In light of the role of SR in neurotoxicity, drugs that curb D-serine synthesis may be useful to treat neurodegenerative diseases. A number of SR inhibitors have been employed to demonstrate a role of SR in synthesizing D-serine and regulating NMDAR-dependent physiological processes. Early papers used a general inhibitor of PLP-dependent enzymes, like aminooxyacetic acid (Wolosker et al. 1999b) or L-serine *O*-sulfate, an artificial substrate for α, β-elimination that blocks D-serine synthesis by replacing the natural substrate L-serine (Panizzutti et al. 2001). Subsequent studies employed phenazine and phenazine derivatives to block SR-mediated granule cell migration in the developing cerebellum (Kim et al. 2005). Furthermore, Konvalika and co-workers found that some dicarboxylic substrate analogs are high-affinity competitive SR inhibitors (Strisovsky et al. 2005). These include malonate and L-erythro-3-hydroxyaspartate that work in the micromolar range. The latter was recently employed to demonstrate the role of astrocytic D-serine in regulating hippocampal LTP (Henneberger et al. 2010). Nevertheless, there is no data on the selectivity of any SR inhibitor, and their use to study complex physiological processes, like neurotransmission, should be avoided, unless SR knockout (KO) mice or shRNA strategy can be used as controls to ensure the inhibitor specificity toward SR. The recent description of SR structure and the availability of in silico screening and docking approaches will facilitate the development of more selective inhibitors.

Serine racemase-knockout mouse strains

The development of SR-KO mice was crucial to clarify the physiological and pathological roles of SR. To date, three SR-KO mouse strains have been developed (Inoue et al. 2008; Basu et al. 2009; Labrie et al. 2009) (Table 1). The first SR-KO mouse strain was generated by homologous recombination in embryonic stem (ES) cells derived from the C57BL/6 strain, and the resulting insertional mutation-type SR-KO mice therefore have a pure C57BL/6 genetic background suitable for the analysis of brain functions (Miya et al. 2008). This strain is now referred to as SR-KO^{HM}. The second, flox-type, SR-KO mouse strain was generated by homologous recombination in 129Sv-derived ES cells and backcrossed with the C57BL/6 strain (Basu et al. 2009). This strain is referred to as SR-KO^{JTC}. The third SR-KO mouse strain was identified from the F1 progeny of ethylnitrosourea (ENU)-mutagenized C57BL/6 male mice and DBA/2 female mice (Labrie et al. 2009). The ENU-induced mutation was identified as a nonsense mutation resulting in the conversion of tyrosine 269 of the SR protein to a stop codon (SrrY269* strain). The F1 founder carrying the SrrY269* mutation was backcrossed with the C57BL/6 strain. The main difference among these mouse strains is their genetic background. Recently, cell-type selective conditional SR-KO mice, namely, astrocyte-selective SR conditional knockout (aSR-KO^{JTC}) and forebrain glutamatergic neuron-selective SR knockout (nSR-KO^{JTC}) mice have been reported (Benneyworth et al. 2012).

Production of D-serine catalyzed by SR in vivo

The three strains of SR-KO mice show no detectable SR protein, and their brain D-serine levels are 10–20 % of the wild-type (WT) controls. The levels of L-serine, glycine

Table 1 Summary of phenotypes of three SR-KO mouse strains

Strains	SR-KO^{HM}	SR-KO^{JTC}	SrrY269*
Genetic background	C57BL/6	129 Sv ES derived × C57BL/6 (N7)	C57BL/6 ENU mutagenesis × DBA derived × C57BL/6 (N8)
Biochemical changes			
SR protein	No	No	No
D-Ser	Reduced (10 % of WT)	Reduced (10 %)	Reduced (10–20 %)
L-Ser	No change	No change	Increased (frontal cortex)
NMDAR activity	Reduced (excitotoxicity assay)	Reduced (electrophysiology)	Not tested
Behavioral tests			
PPI	No change	No change	Impaired
Locomotion	No change	Enhanced (male)	No change
Learning and Memory	Impaired (contextual learning)	Impaired (Morris water maze)	Impaired (Morris water maze)

and glutamate in the cerebral cortex of SR-KO^{HM} and SR-KO^{JTC} mice are equivalent to those of WT controls (Inoue et al. 2008; Basu et al. 2009), though one study reported higher L-serine levels in the frontal cortex of SrrY269* mice (Labrie et al. 2009). These findings indicate that D-serine production in the mouse brain is predominantly catalyzed by SR (Table 1).

The origin of the residual 10–20 % of D-serine is not known. Conceivably, residual D-serine may originate in peripheral tissues. Specific expression of SR was detected in the liver using SR-KO^{HM} mice as negative controls (Horio et al. 2011). SR-KO^{HM} mice display reduced levels of D-serine in some peripheral organs like the kidney, muscle and testis. However, the levels of D-serine in the liver, spleen, pancreas, epididymis, heart, lung and eye of SR-KO^{HM} mice are comparable to those in WT mice (Horio et al. 2011). Possible alternative pathways for D-serine synthesis include the glycine cleavage system (Iwama et al. 1997), the hydrolysis of phosphoserine by phosphoserine phosphatase (Wood et al. 1996) or exogenous D-serine from intestinal bacterial flora.

Localization of SR in vivo

To fully clarify the role of D-serine in the brain, it is important to precisely define the cellular localizations of SR and D-serine. Early data on SR distribution indicated that the enzyme was glial (Wolosker et al. 1999a). However, subsequent immunohistochemical and in situ hybridization studies revealed the localization of the SR protein (Kartvelishvily et al. 2006) and its mRNA (Yoshikawa et al. 2007) primarily in neurons. More definitive data on SR distribution was obtained using SR-KO^{HM} mice as negative controls (Miya et al. 2008). This approach ensured the specificity of the antibodies and revealed that SR was predominantly localized in pyramidal neurons of the cerebral cortex and hippocampal CA1 region. Double-immunofluorescence experiments revealed that SR colocalizes with neuron-specific nuclear protein (NeuN), but not with astrocytic markers, namely, glial fibrillary acidic protein (GFAP) and 3-phosphoglycerate dehydrogenase (Phgdh). In the striatum, SR is expressed by γ-aminobutyric acid (GABA)ergic medium spiny neurons. Furthermore, in the adult cerebellum, weak but significant SR signals are detected in GABAergic Purkinje cells. The data indicate that SR is expressed by the main neuronal populations in most brain regions, irrespective of the excitatory or inhibitory nature of the cells. Therefore, neurons are likely to be the main source of D-serine (Miya et al. 2008). These results, however, cannot exclude the possibility of SR expression in glial cells in vivo at levels below the sensitivity of the available antibodies. In primary cultured cells, SR is expressed in both neurons and astrocytes at similar levels, indicating that the pattern of SR expression in astrocytes in vitro differs from that observed in vivo.

Recently, the notion that SR is predominantly neuronal gathered additional support from the analysis of nSR-KO^{JTC} mice. These mice exhibit lower D-serine and SR expression in the brain, especially in cortical glutamatergic neurons (Benneyworth et al. 2012). Astrocyte-specific SR-KO mice (aSR-KO^{JTC}) exhibit no change in D-serine levels. Notably, the decrease in SR expression observed in nSR-KO^{JTC} mice (about 60 % in the cortex) was more prominent than the decrease in D-serine by HPLC (around 30 % decrease). While these results underscore the importance of neurons in synthesizing D-serine (Benneyworth et al. 2012), they raise additional questions regarding possible alternative sources of D-serine. D-Serine crosses the blood–brain barrier and it is possible that some of brain D-serine comes from the periphery. SR expression in the liver is upregulated in nSR-KO^{JTC} mice, suggesting that

there may be a "cross talk" between the brain and the liver that maintains peripheral and brain D-serine levels (Benneyworth et al. 2012).

Morphological features of brain of SR-KO mice

SR-KO^{JTC} mice display reduced cortical volume (Balu et al. 2012). Neurons in the medial prefrontal cortex (PFC) of SR-KO^{JTC} mice show reduced complexity, total length and spine density of apical dendrites (DeVito et al. 2011). Furthermore, pyramidal neurons in the primary somatosensory cortex (S1) of SR-KO^{JTC} mice also show reduced complexity, total length and spine density of apical and basal dendrites (Balu et al. 2012). However, the gross formation and patterning of barrels in the posteriomedial barrel subfield in S1 are normal. Decreased expression of brain-derived neurotrophic factor (BDNF) may be associated with these morphological changes (Balu et al. 2012).

Gene expression in SR-KO mice

The expression levels of various proteins were analyzed in SR-KO mice, and the observed changes may reflect adaptations to NMDAR hypofunction. The expression of NMDAR subunits, namely, GluN1, GluN2A and GluN2B, which are abundant in the forebrain, are the same in brain homogenates of WT and SR-KO mice (Inoue et al. 2008; Labrie et al. 2009). In contrast, SR-KO^{JTC} mice displayed higher levels of GluN1 and GluN2A subunit expression in postsynaptic density (PSD) fractions obtained from hippocampus, though the levels of these receptors in PFC of SR-KO^{JTC} mice were unaltered (Balu and Coyle 2011). The expression levels of other GluN2B and PSD-95 proteins were unchanged in the PSD fraction from SR-KO^{JTC} mice. Furthermore, another study reported higher expression of GluN1 subunit in the striatum of SR-KO^{JTC} mice (Mustafa et al. 2010). These observed increases in NMDAR subunits may reflect synaptic adaptations to compensate for presumed lower NMDAR activation in SR-KO, but an effect due to differences in genetic backgrounds of the KO mouse strains cannot be ruled out. The differences described above in the expression of glutamate receptors were not observed in all SR-KO strains. For instance, SR-KO^{HM} mice made in pure C57BL/6 background display no changes in striatal GluN1 subunit protein (Inoue, R., Imai-Tabata, A. and H. M, unpublished results).

The expression levels of AMPARs GluA1 and GluA2 subunits, D-amino acid oxidase and glycine transporter 1 (GlyT1) remained unchanged in the whole-brain SrrY269* homogenates (Labrie et al. 2009). In contrast, SrrY269* overexpress the PICK1, which binds to the carboxy terminus of mouse SR (Labrie et al. 2009). A combination of DNA microarray experiments, RT-PCR and Western blot analysis revealed higher expression of transthyretin, ectonucleotide pyrophosphatase/phosphodiesterase 2, klotho, insulin-like growth factor 2, prolactin receptor and claudin 2 proteins in SrrY269* mice (Labrie et al. 2009). The physiological significance of the increases in the expression levels of these proteins remains unknown.

Some genes were expressed at lower levels in SR-KO, and their reduction might contribute to the phenotype. Notably, SR-KO^{JTC} mice display reduced expression of BDNF protein. Lower BDNF expression provides a possible explanation for the morphological changes in dendritic structure of neurons in the somatosensory cortex observed in the SR-KO^{JTC} mice (Balu et al. 2012).

Neurotransmission in SR-KO mice

Analyses of neurotransmission between Schaffer collateral and hippocampal CA1 by whole-cell patch-clamp recording from brain slices of juvenile (postnatal days 21–28) SR-KO mice revealed slower decay kinetics of NMDAR-mediated excitatory postsynaptic potentials (EPSPs), suggesting a contribution of the GluN2B subunit containing NMDAR in SR-KO^{JTC} mice (Basu et al. 2009). This observation is supported by the higher GluN2B protein expression detected in juvenile SR-KO^{JTC} mice brains (Balu and Coyle 2011). Expression of hippocampal synaptic plasticity was also altered in SR-KO^{JTC} mice. The NMDAR-dependent long-term potentiation (LTP) of synaptic transmission induced using a pairing stimulation protocol is impaired in juvenile SR-KO^{JTC} mice (Basu et al. 2009). The impairment of LTP induction can be rescued using bath-applied D-serine. In contrast to these phenotypes of neurotransmission in juvenile SR-KO^{JTC} mice, we have not detected impairment of neurotransmission in hippocampal CA1 synapses of adult mice in a recent study using SR-KO^{HM} (Watanabe, M., H. M. and Manabe, T., unpublished results).

In the nSR-KO^{JTC} mice, NMDAR-mediated EPSPs were reduced and LTP induction by weak single train tetanus protocol was lower than in WT control mice. In contrast, LTP induced with a strong three-train protocol was comparable to that of WT mice (Benneyworth et al. 2012). These data support the notion that neuron-derived D-Serine regulates synaptic plasticity.

D-Serine is present in the retina, though at levels 20-fold lower than those of L-serine (Sullivan et al. 2011). Whole-cell recordings from SR-KO^{JTC} retinal ganglion cells lack light-evoked NMDAR currents. In contrast to the attenuated NMDAR responses detected by electrophysiological analysis, no obvious visual impairment was observed in

behavioral tests (Sullivan et al. 2011). Though SR and D-serine were initially reported to be exclusively localized to glial Muller cells, subsequent studies showed robust SR expression by ganglion cells, supporting a possible role of neuron-derived D-serine in the retina as well (Dun et al. 2008).

Additional biochemical evidence supporting lower NMDAR activation in SR-KO comes from nitrosylation studies. SR-KO^{JTC} display lower levels of nitrosylation of known nitrosylation targets, a process known to be dependent on NOS activity via NMDAR activation (Mustafa et al. 2010).

Behaviors of SR-KO mice

NMDARs are involved in learning and memory, and these processes have been studied using the Morris water maze paradigm which assesses hippocampal NMDAR-dependent spatial memory (Morris et al. 1986). SR-KO^{JTC} and SrrY269* male mice show an impaired spatial reference memory, indicating a role of D-serine in spatial discrimination (Basu et al. 2009; Labrie et al. 2009). Likewise, SR-KO^{HM} also exhibited impaired contextual learning (Inoue,R. and H.M., unpublished observation). SR-KO^{JTC} mice exhibit disrupted representation of the odor associated with events in distinct experiences monitored by object recognition and the odor sequence test (DeVito et al. 2011). On the other hand, SR-KO^{JTC} mice showed intact relational memory in a test of transitive inference, and displayed normal behaviors in the detection of novel objects and in spatial displacement tasks (DeVito et al. 2011). These findings were correlated to altered dendritic morphology and lower spine density in pyramidal neurons of the prefrontal cortex. Altogether, these observations indicate that D-serine is required for cognitive ability.

SR-KO^{JTC} mice show normal motor coordination and no evidence of anxiety or depression-like behaviors (Basu et al. 2009; Labrie et al. 2009). Male SR-KO^{JTC} mice show increased locomotor activity (Basu et al. 2009). The effects of SR-KO on other sexually dimorphic phenotypes in behavioral assays reported by Basu et al. remain to be determined.

Prepulse inhibition (PPI) of the acoustic startle response (ASR) is one indication of the sensory–motor gating process, and is inhibited by the pharmacological suppression of NMDAR. Inhibition of PPI is also observed in patients with schizophrenia (Cadenhead et al. 2000). Despite data indicating reduced NMDAR function, no consistent inhibition of PPI was observed in SR-KO mice, as the effects were strain specific. One study found no difference in PPI between WT and SR-KO^{HM} mice (Mori and Inoue 2010). Basu et al. (2009) also reported the absence of PPI deficit in SR-KO^{JTC} mice, although they observed elevated ASR in female SR-KO mice. In contrast, SrrY269* mice showed diminished PPI; however, under the same conditions, control mice showed no enhancement of PPI with the increase in the prepulse tones (Labrie et al. 2009).

The effects of psychotomimetic drugs, such as phencyclidine (PCP) and amphetamine (AMPH) as well as methamphetamine (METH), on locomotor activity and sensory-motor gating were also examined in SR-KO mice in the context of PPI. Acute PCP-enhanced startle reactivity was increased in SR-KO^{JTC} mice, but AMPH effects were similar to those of WT mice (Benneyworth et al. 2011). Repeated administration of METH results in behavioral sensitization in WT mice, but not in SR-KO^{HM} mice (Horio et al. 2012). This effect was accompanied by lower METH-induced dopamine release in the nucleus accumbens along with decreased METH-induced phosphorylation of ERK1/2 in the striatum of SR-KO^{HM} mice (Horio et al. 2012).

Altogether, the data indicate that SR-KO shows signs of NMDAR hypofunction in many behavioral paradigms, but the effects seem to vary depending on the genetic background of the strain of mice used (Table 1).

Neurodegeneration in SR-KO mice

SR-KO mice display less susceptibility to excitotoxic insults in several models of neurodegeneration, indicating a role of endogenous D-serine in mediating NMDAR-dependent neurotoxicity. Injection of NMDA in the cerebral cortex induces excitotoxic neuronal cell death, and this effect was attenuated in SR-KO^{HM} mice (Inoue et al. 2008). SR-KO^{HM} mice are also resistant to Aβ peptide-mediated neurodegeneration in vivo, an experimental model relevant to Alzheimer disease (Suh and Checler 2002). Injection of Aβ 1–42 peptide into the hippocampus caused significantly less damage in SR-KO^{HM} mice (Inoue et al. 2008). Aβ-induced neurotoxicity was mostly dependent on the function of the NMDAR, because the damage by Aβ was prevented by pretreatment with the NMDAR antagonist MK-801. These results implicate D-serine in neurodegeneration (Inoue et al. 2008). Furthermore, infarct volume following middle cerebral artery occlusion is significantly reduced in SR-KO^{JTC} mice (Mustafa et al. 2010). Together with previous data using brain slices in vitro which showed that D-serine might be the dominant co-agonist for NMDAR-mediated excitotoxicity (Katsuki et al. 2004; Shleper et al. 2005), the results clearly demonstrate that D-serine plays a role in neurodegeneration. This has implications for neurodegenerative diseases in which NMDARs overstimulation leads to neuronal death, such as Huntington and Alzheimer disease. The prominent

role of D-serine in neurotoxicity is consistent with the notion that D-serine availability is a fail-safe mechanism to prevent excessive NMDAR activity during increases in glutamatergic neurotransmission.

Is D-serine a gliotransmitter?

Several studies indicate that D-serine may be released from glia and function as a "gliotransmitter" to regulate NMDAR transmission and synaptic plasticity. This notion is supported by the presence of D-serine in glia (Schell et al. 1995, 1997; Williams et al. 2006), especially in vesicular structures (Bergersen et al. 2011; Mothet et al. 2005; Williams et al. 2006) that undergo exocytosis upon glutamate receptor stimulation (Mothet et al. 2005). Furthermore, Mothet and co-workers demonstrated that the Ca^{2+}-dependent D-serine pool corresponds to vesicles of the secretory pathway in astrocytes (Martineau et al. 2008). Based on these data, previous electrophysiological effects of endogenous D-serine on NMDARs were mostly interpreted as evidence for gliotransmission (Mothet et al. 2000; Henneberger et al. 2010; Panatier et al. 2006; Yang et al. 2003, 2005). The gliotransmitter hypothesis is still somewhat controversial, as there is no specific pharmacological approach that interferes with glial metabolism or transmitter release without having indirect effects on neuronal metabolism or physiology (Agulhon et al. 2008, 2010). Furthermore, non-vesicular release of D-serine and glutamate from glia has been demonstrated (O'Brien and Bowser 2006; Ribeiro et al. 2002; Rosenberg et al. 2010). The recent data showing that neurons can be a source for D-serine release, and that SR is predominantly localized in neurons (Kartvelishvily et al. 2006; Rosenberg et al. 2010; Benneyworth et al. 2011; Miya et al. 2008), raise further questions regarding the relative roles of neurons versus glia in releasing D-serine. Future studies employing more selective pharmacologic or genetic approaches will be required to differentiate between glia- and neuron-derived D-serine. In any case, a substantial number of existing pharmacologic and genetic models indicate that D-serine is required for optimal NMDAR function and opens new possibilities for developing drugs to modulate NMDAR function.

Acknowledgments We thank Dr. Ran Inoue and Jeffrey Ehmsen for critical reading of the manuscript. Work in H.W. laboratory was supported by grants from IMHRO, Israel Science Foundation, ISF-Legacy Heritage Fund, Jessie Kaplan Research Fund, Dears Foundation, L. Aronberg Research Fund in Neurology and Albert Goodstein Research Fund. H.M. was supported by a grant from the Ministry of Education, Culture, Sports, Science, and Technology of Japan (Grant No. 221S0003).

References

Agulhon C, Petravicz J, McMullen AB, Sweger EJ, Minton SK, Taves SR, Casper KB, Fiacco TA, McCarthy KD (2008) What is the role of astrocyte calcium in neurophysiology? Neuron 59(6):932–946. doi:10.1016/j.neuron.2008.09.004

Agulhon C, Fiacco TA, McCarthy KD (2010) Hippocampal short- and long-term plasticity are not modulated by astrocyte Ca2+ signaling. Science 327(5970):1250–1254. doi:10.1126/science.1184821

Balan L, Foltyn VN, Zehl M, Dumin E, Dikopoltsev E, Knoh D, Ohno Y, Kihara A, Jensen ON, Radzishevsky IS, Wolosker H (2009) Feedback inactivation of D-serine synthesis by NMDA receptor-elicited translocation of serine racemase to the membrane. Proc Natl Acad Sci USA 106(18):7589–7594

Balu DT, Coyle JT (2011) Glutamate receptor composition of the post-synaptic density is altered in genetic mouse models of NMDA receptor hypo- and hyperfunction. Brain Res 1392:1–7. doi:10.1016/j.brainres.2011.03.051

Balu DT, Basu AC, Corradi JP, Cacace AM, Coyle JT (2012) The NMDA receptor co-agonists, D-serine and glycine, regulate neuronal dendritic architecture in the somatosensory cortex. Neurobiol Dis 45(2):671–682. doi:10.1016/j.nbd.2011.10.006

Basu AC, Tsai GE, Ma CL, Ehmsen JT, Mustafa AK, Han L, Jiang ZI, Benneyworth MA, Froimowitz MP, Lange N, Snyder SH, Bergeron R, Coyle JT (2009) Targeted disruption of serine racemase affects glutamatergic neurotransmission and behavior. Molecular psychiatry 14(7):719–727. doi:10.1038/mp.2008.130

Baumgart F, Mancheno JM, Rodriguez-Crespo I (2007) Insights into the activation of brain serine racemase by the multi-PDZ domain glutamate receptor interacting protein, divalent cations and ATP. FEBS J 274(17):4561–4571

Benneyworth MA, Basu AC, Coyle JT (2011) Discordant behavioral effects of psychotomimetic drugs in mice with altered NMDA receptor function. Psychopharmacology (Berl) 213(1):143–153. doi:10.1007/s00213-010-2023-4

Benneyworth MA, Li Y, Basu AC, Bolshakov VY, Coyle JT (2012) Cell selective conditional null mutations of serine racemase demonstrate a predominate localization in cortical glutamatergic neurons. Cell Mol Neurobiol 32(4):613–624. doi:10.1007/s10571-012-9808-4

Bergersen LH, Morland C, Ormel L, Rinholm JE, Larsson M, Wold JF, Roe AT, Stranna A, Santello M, Bouvier D, Ottersen OP, Volterra A, Gundersen V (2011) Immunogold detection of L-glutamate and D-serine in small synaptic-like microvesicles in adult hippocampal astrocytes. Cereb Cortex. doi:10.1093/cercor/bhr254

Cadenhead KS, Swerdlow NR, Shafer KM, Diaz M, Braff DL (2000) Modulation of the startle response and startle laterality in relatives of schizophrenic patients and in subjects with schizotypal personality disorder: evidence of inhibitory deficits. Am J Psychiatry 157(10):1660–1668

Cook SP, Galve-Roperh I, Martinez Del Pozo A, Rodriguez-Crespo I (2002) Direct calcium binding results in activation of brain serine racemase. J Biol Chem 277(31):27782–27792

De Miranda J, Santoro A, Engelender S, Wolosker H (2000) Human serine racemase: molecular cloning, genomic organization and functional analysis. Gene 256(1–2):183–188

De Miranda J, Panizzutti R, Foltyn VN, Wolosker H (2002) Cofactors of serine racemase that physiologically stimulate the synthesis of the *N*-methyl-D-aspartate (NMDA) receptor coagonist D-serine. Proc Natl Acad Sci USA 99(22):14542–14547

DeVito LM, Balu DT, Kanter BR, Lykken C, Basu AC, Coyle JT, Eichenbaum H (2011) Serine racemase deletion disrupts memory

for order and alters cortical dendritic morphology. Genes Brain Behav 10(2):210–222. doi:10.1111/j.1601-183X.2010.00656.x

Dumin E, Bendikov I, Foltyn VN, Misumi Y, Ikehara Y, Kartvelishvily E, Wolosker H (2006) Modulation of D-serine levels via ubiquitin-dependent proteasomal degradation of serine racemase. J Biol Chem 281(29):20291–20302

Dun Y, Duplantier J, Roon P, Martin PM, Ganapathy V, Smith SB (2008) Serine racemase expression and D-serine content are developmentally regulated in neuronal ganglion cells of the retina. J Neurochem 104(4):970–978. doi:10.1111/j.1471-4159.2007.05015.x

Dunlop DS, Neidle A (1997) The origin and turnover of D-serine in brain. Biochem Biophys Res Commun 235(1):26–30

Dunlop DS, Neidle A (2005) Regulation of serine racemase activity by amino acids. Brain Res Mol Brain Res 133(2):208–214

Foltyn VN, Bendikov I, De Miranda J, Panizzutti R, Dumin E, Shleper M, Li P, Toney MD, Kartvelishvily E, Wolosker H (2005) Serine racemase modulates intracellular D-serine levels through an alpha, beta-elimination activity. J Biol Chem 280(3):1754–1763

Foltyn VN, Zehl M, Dikopoltsev E, Jensen ON, Wolosker H (2010) Phosphorylation of mouse serine racemase regulates D-serine synthesis. FEBS Lett 584(13):2937–2941

Fujii K, Maeda K, Hikida T, Mustafa AK, Balkissoon R, Xia J, Yamada T, Ozeki Y, Kawahara R, Okawa M, Huganir RL, Ujike H, Snyder SH, Sawa A (2006) Serine racemase binds to PICK1: potential relevance to schizophrenia. Mol Psychiatry 11(2):150–157

Goto M, Yamauchi T, Kamiya N, Miyahara I, Yoshimura T, Mihara H, Kurihara T, Hirotsu K, Esaki N (2009) Crystal structure of a homolog of mammalian serine racemase from Schizosaccharomyces pombe. J Biol Chem 284(38):25944–25952

Hashimoto A, Nishikawa T, Oka T, Takahashi K, Hayashi T (1992) Determination of free amino acid enantiomers in rat brain and serum by high-performance liquid chromatography after derivatization with *N*-tert.-butyloxycarbonyl-L-cysteine and *o*-phthaldialdehyde. J Chromatogr 582(1–2):41–48

Hashimoto A, Nishikawa T, Konno R, Niwa A, Yasumura Y, Oka T, Takahashi K (1993) Free D-serine, D-aspartate and D-alanine in central nervous system and serum in mutant mice lacking D-amino acid oxidase. Neurosci Lett 152(1–2):33–36

Henneberger C, Papouin T, Oliet SH, Rusakov DA (2010) Long-term potentiation depends on release of D-serine from astrocytes. Nature 463(7278):232–236

Hikida T, Mustafa AK, Maeda K, Fujii K, Barrow RK, Saleh M, Huganir RL, Snyder SH, Hashimoto K, Sawa A (2008) Modulation of D-serine levels in brains of mice lacking PICK1. Biol Psychiatry 63(10):997–1000

Horio M, Kohno M, Fujita Y, Ishima T, Inoue R, Mori H, Hashimoto K (2011) Levels of D-serine in the brain and peripheral organs of serine racemase (Srr) knock-out mice. Neurochem Int 59(6):853–859. doi:10.1016/j.neuint.2011.08.017

Horio M, Kohno M, Fujita Y, Ishima T, Inoue R, Mori H, Hashimoto K (2012) Role of serine racemase in behavioral sensitization in mice after repeated administration of methamphetamine. PLoS One 7(4):e35494. doi:10.1371/journal.pone.0035494

Huttlin EL, Jedrychowski MP, Elias JE, Goswami T, Rad R, Beausoleil SA, Villen J, Haas W, Sowa ME, Gygi SP (2010) A tissue-specific atlas of mouse protein phosphorylation and expression. Cell 143(7):1174–1189. doi:10.1016/j.cell.2010.12.001

Inoue R, Hashimoto K, Harai T, Mori H (2008) NMDA- and beta-amyloid1-42-induced neurotoxicity is attenuated in serine racemase knock-out mice. J Neurosci 28(53):14486–14491. doi:10.1523/JNEUROSCI.5034-08.2008

Iwama H, Takahashi K, Kure S, Hayashi F, Narisawa K, Tada K, Mizoguchi M, Takashima S, Tomita U, Nishikawa T (1997) Depletion of cerebral D-serine in non-ketotic hyperglycinemia: possible involvement of glycine cleavage system in control of endogenous D-serine. Biochem Biophys Res Commun 231(3):793–796. doi:10.1006/bbrc.1997.6184

Kartvelishvily E, Shleper M, Balan L, Dumin E, Wolosker H (2006) Neuron-derived D-serine release provides a novel means to activate *N*-methyl-D-aspartate receptors. J Biol Chem 281(20):14151–14162

Katsuki H, Nonaka M, Shirakawa H, Kume T, Akaike A (2004) Endogenous D-serine is involved in induction of neuronal death by *N*-methyl-D-aspartate and simulated ischemia in rat cerebrocortical slices. J Pharmacol Exp Ther 311(2):836–844

Kim PM, Aizawa H, Kim PS, Huang AS, Wickramasinghe SR, Kashani AH, Barrow RK, Huganir RL, Ghosh A, Snyder SH (2005) Serine racemase: activation by glutamate neurotransmission via glutamate receptor interacting protein and mediation of neuronal migration. Proc Natl Acad Sci USA 102(6):2105–2110

Konno R (2003) Rat cerebral serine racemase: amino acid deletion and truncation at carboxy terminus. Neurosci Lett 349(2):111–114

Labrie V, Fukumura R, Rastogi A, Fick LJ, Wang W, Boutros PC, Kennedy JL, Semeralul MO, Lee FH, Baker GB, Belsham DD, Barger SW, Gondo Y, Wong AH, Roder JC (2009) Serine racemase is associated with schizophrenia susceptibility in humans and in a mouse model. Hum Mol Genet 18(17):3227–3243

Martineau M, Galli T, Baux G, Mothet JP (2008) Confocal imaging and tracking of the exocytotic routes for D-serine-mediated gliotransmission. Glia 56:1271–1284. doi:10.1002/glia.20696

Miya K, Inoue R, Takata Y, Abe M, Natsume R, Sakimura K, Hongou K, Miyawaki T, Mori H (2008) Serine racemase is predominantly localized in neurons in mouse brain. J Comp Neurol 510(6):641–654. doi:10.1002/cne.21822

Mori H, Inoue R (2010) Serine racemase knockout mice. Chem Biodivers 7(6):1573–1578. doi:10.1002/cbdv.200900293

Morris RG, Anderson E, Lynch GS, Baudry M (1986) Selective impairment of learning and blockade of long-term potentiation by an *N*-methyl-D-aspartate receptor antagonist, AP5. Nature 319(6056):774–776. doi:10.1038/319774a0

Mothet JP, Parent AT, Wolosker H, Brady RO Jr, Linden DJ, Ferris CD, Rogawski MA, Snyder SH (2000) D-serine is an endogenous ligand for the glycine site of the *N*-methyl-D-aspartate receptor. Proc Natl Acad Sci USA 97(9):4926–4931

Mothet JP, Pollegioni L, Ouanounou G, Martineau M, Fossier P, Baux G (2005) Glutamate receptor activation triggers a calcium-dependent and SNARE protein-dependent release of the gliotransmitter D-serine. Proc Natl Acad Sci USA 102(15):5606–5611

Mustafa AK, Kumar M, Selvakumar B, Ho GP, Ehmsen JT, Barrow RK, Amzel LM, Snyder SH (2007) Nitric oxide S-nitrosylates serine racemase, mediating feedback inhibition of D-serine formation. Proc Natl Acad Sci USA 104(8):2950–2955

Mustafa AK, van Rossum DB, Patterson RL, Maag D, Ehmsen JT, Gazi SK, Chakraborty A, Barrow RK, Amzel LM, Snyder SH (2009) Glutamatergic regulation of serine racemase via reversal of PIP2 inhibition. Proc Natl Acad Sci USA 106(8):2921–2926

Mustafa AK, Ahmad AS, Zeynalov E, Gazi SK, Sikka G, Ehmsen JT, Barrow RK, Coyle JT, Snyder SH, Dore S (2010) Serine racemase deletion protects against cerebral ischemia and excitotoxicity. J Neurosci 30(4):1413–1416

Nagata Y, Homma H, Matsumoto M, Imai K (1999) Stimulation of steroidogenic acute regulatory protein (StAR) gene expression by D-aspartate in rat Leydig cells. FEBS Lett 454(3):317–320

Neidle A, Dunlop DS (2002) Allosteric regulation of mouse brain serine racemase. Neurochem Res 27(12):1719–1724

Nishikawa T (2005) Metabolism and functional roles of endogenous D-serine in mammalian brains. Biol Pharm Bull 28(9): 1561–1565

O'Brien KB, Bowser MT (2006) Measuring D-serine efflux from mouse cortical brain slices using online microdialysis-capillary electrophoresis. Electrophoresis 27(10):1949–1956

Panatier A, Theodosis DT, Mothet JP, Touquet B, Pollegioni L, Poulain DA, Oliet SH (2006) Glia-derived D-serine controls NMDA receptor activity and synaptic memory. Cell 125(4): 775–784

Panizzutti R, De Miranda J, Ribeiro CS, Engelender S, Wolosker H (2001) A new strategy to decrease *N*-methyl-D-aspartate (NMDA) receptor coactivation: inhibition of D-serine synthesis by converting serine racemase into an eliminase. Proc Natl Acad Sci USA 98(9):5294–5299

Ribeiro CS, Reis M, Panizzutti R, de Miranda J, Wolosker H (2002) Glial transport of the neuromodulator D-serine. Brain Res 929(2):202–209

Rosenberg D, Kartvelishvily E, Shleper M, Klinker CM, Bowser MT, Wolosker H (2010) Neuronal release of D-serine: a physiological pathway controlling extracellular D-serine concentration. FASEB J 24(8):2951–2961

Schell MJ, Molliver ME, Snyder SH (1995) D-serine, an endogenous synaptic modulator: localization to astrocytes and glutamate-stimulated release. Proc Natl Acad Sci USA 92(9):3948–3952

Schell MJ, Brady RO Jr, Molliver ME, Snyder SH (1997) D-serine as a neuromodulator: regional and developmental localizations in rat brain glia resemble NMDA receptors. J Neurosci 17(5):1604–1615

Shleper M, Kartvelishvily E, Wolosker H (2005) D-serine is the dominant endogenous coagonist for NMDA receptor neurotoxicity in organotypic hippocampal slices. J Neurosci 25(41): 9413–9417

Smith MA, Mack V, Ebneth A, Moraes I, Felicetti B, Wood M, Schonfeld D, Mather O, Cesura A, Barker J (2010) The structure of mammalian serine racemase: evidence for conformational changes upon inhibitor binding. J Biol Chem 285(17): 12873–12881

Strisovsky K, Jiraskova J, Mikulova A, Rulisek L, Konvalinka J (2005) Dual substrate and reaction specificity in mouse serine racemase: identification of high-affinity dicarboxylate substrate and inhibitors and analysis of the beta-eliminase activity. Biochemistry 44(39):13091–13100

Suh YH, Checler F (2002) Amyloid precursor protein, presenilins, and alpha-synuclein: molecular pathogenesis and pharmacological applications in Alzheimer's disease. Pharmacol Rev 54(3): 469–525

Sullivan SJ, Esguerra M, Wickham RJ, Romero GE, Coyle JT, Miller RF (2011) Serine racemase deletion abolishes light-evoked NMDA receptor currents in retinal ganglion cells. J Physiol 589(Pt 24):5997–6006. doi:10.1113/jphysiol.2011.217059

Takahashi K, Hayashi F, Nishikawa T (1997) In vivo evidence for the link between L- and D-serine metabolism in rat cerebral cortex. J Neurochem 69(3):1286–1290

Uo T, Yoshimura T, Shimizu S, Esaki N (1998) Occurrence of pyridoxal 5′-phosphate-dependent serine racemase in silkworm *Bombyx mori*. Biochem Biophys Res Commun 246(1):31–34

Williams SM, Diaz CM, Macnab LT, Sullivan RK, Pow DV (2006) Immunocytochemical analysis of D-serine distribution in the mammalian brain reveals novel anatomical compartmentalizations in glia and neurons. Glia 53(4):401–411

Wisniewski JR, Nagaraj N, Zougman A, Gnad F, Mann M (2010) Brain phosphoproteome obtained by a FASP-based method reveals plasma membrane protein topology. J Proteome Res 9(6):3280–3289. doi:10.1021/pr1002214

Wolosker H (1814) (2011) Serine racemase and the serine shuttle between neurons and astrocytes. Biochim Biophys Acta 1814(11):1558–1566

Wolosker H, Blackshaw S, Snyder SH (1999a) Serine racemase: a glial enzyme synthesizing D-serine to regulate glutamate-*N*-methyl-D-aspartate neurotransmission. Proc Nat Acad Sci USA 96(23):13409–13414

Wolosker H, Sheth KN, Takahashi M, Mothet JP, Brady RO Jr, Ferris CD, Snyder SH (1999b) Purification of serine racemase: biosynthesis of the neuromodulator D-serine. Proc Natl Acad Sci USA 96(2):721–725

Wood PL, Hawkinson JE, Goodnough DB (1996) Formation of D-serine from L-phosphoserine in brain synaptosomes. J Neurochem 67(4):1485–1490

Yang Y, Ge W, Chen Y, Zhang Z, Shen W, Wu C, Poo M, Duan S (2003) Contribution of astrocytes to hippocampal long-term potentiation through release of D-serine. Proc Natl Acad Sci USA 100(25):15194–15199

Yang S, Qiao H, Wen L, Zhou W, Zhang Y (2005) D-Serine enhances impaired long-term potentiation in CA1 subfield of hippocampal slices from aged senescence-accelerated mouse prone/8. Neurosci Lett 379(1):7–12

Yoshikawa M, Takayasu N, Hashimoto A, Sato Y, Tamaki R, Tsukamoto H, Kobayashi H, Noda S (2007) The serine racemase mRNA is predominantly expressed in rat brain neurons. Arch Histol Cytol 70(2):127–134

Bioconjugate Chemistry

ARTICLE

pubs.acs.org/bc

Real-Time Monitoring of Actin Polymerization in Living Cells Using Split Luciferase

Tetsuya Ishimoto,[†] Takeaki Ozawa,[‡,§] and Hisashi Mori*[,†]

[†]Department of Molecular Neuroscience, Graduate School of Medicine and Pharmaceutical Sciences, University of Toyama, Toyama, Japan.

[‡]Department of Chemistry, Graduate School of Science, The University of Tokyo, Bunkyo-Ku, Tokyo, Japan.

[§]Precursory Research for Embryonic Science and Technology, Japan Science and Technology Agency, Tokyo, Japan.

ABSTRACT: Real-time monitoring of actin polymerization in living cells is beneficial for characterizing cellular activities such as migration, proliferation, and death. We developed new bioluminescence-based probe proteins that enable the monitoring of actin polymerization in living cells. Unlike other ordinary split luciferase probes, our probes were incorporated in endogenous actin filament that enabled it to measure the actin polymerization quantitatively. The probe proteins exhibited a dose-responsive decrease in photon emission intensity in response to the filamentous (F)-actin-disrupting agent latrunculin A. This technique has a high sensitivity with a high signal-to-noise ratio and is nontoxic compared with other methods of monitoring actin polymerization in living cells. Using this technique, we succeeded in monitoring the F-actin level in living cells during apoptosis progression induced by UV irradiation continuously for 12 h. F-actin was transiently upregulated after UV irradiation. Since UV-induced cell death was enhanced by treatment with latrunculin A during the period which F-actin is increased, transient upregulation of F-actin after UV is likely a protective reaction against UV-induced cell death. Our novel technique is an effective tool for investigating actin polymerization in living cells.

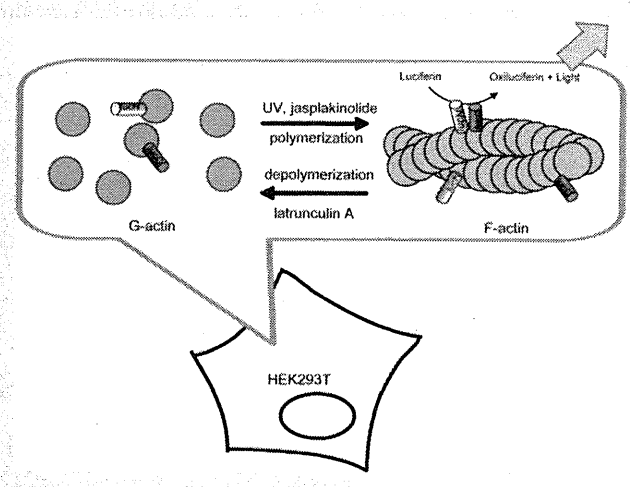

INTRODUCTION

Actin is a major cytoskeletal protein, the sequence of which is highly conserved among all eukaryotes, and is of two dynamic forms, globular (G) actin and its polymerized form, filamentous (F) actin. The organization of F-actin has been considered important for many cellular functions such as migration,[1,2] cancer cell invasion,[3] synaptic plasticity,[4,5] and cell death.[6,7] Measurement of the level of F-actin is important for analyzing cell activity. However, the conventional methods for analyzing F-actin have some limitations. Rhodamine-phalloidin (R-P) staining[8] cannot be used for the long-term and real-time monitoring of F-actin in living cells, since it requires cell fixation. Fluorescent probe proteins such as GFP-actin[9] and lifeact[10] are not suitable for the quantification of F-actin since their monomers can emit fluorescence. Recently, the fluorescence resonance energy transfer (FRET) technique has been used to monitor F-actin,[11] although the FRET signal intensity is not in proportion to the level of F-actin.[12] Furthermore, all the fluorescence-based methods have phototoxicity caused by excitation light. Thus, we tried to develop novel probe proteins to measure the F-actin level in living cells over a long period. The firefly split luciferase technique, which has been developed by several groups in the past decade,[13−15] was employed to develop probe proteins, since bioluminescence-based methods have some advantages in terms of the viability of cells and linearity of signal intensity. In this report, we describe the development of novel probe proteins for monitoring actin polymerization.

To validate the usefulness of our probe proteins, we focused on the regulation of actin polymerization in cell death. The disruption of F-actin induces apoptotic cell death in T cells and MCF10A cells, and enhances apoptosis by cytokine withdrawal in CTLL-20 cells.[16−18] These reports suggest that actin polymerization has a protective role against the cell death. However, few reports have described the detailed time course and quantification of the actin polymerization in cell death due to lack of appropriate method. Using our probe proteins, we attempt to elucidate the precise time course of actin polymerization after cell death stimulus and try to predict the critical period that F-actin works protectively.

EXPERIMENTAL PROCEDURES

Plasmid Construction. A MultiSite Gateway Three-Fragment Vector Construction kit (Invitrogen) was used for plasmid

Received: December 25, 2010
Revised: April 7, 2011
Published: May 18, 2011

construction in accordance with the manual. This method is based on site-specific recombination of DNA fragments.[19,20] Briefly, PCR-fragments flanked by recombination sites were inserted to donor vectors to generate 5′, center, and 3′ entry clones by recombination called BP reaction. These three entry clones were reacted with destination vector to generate expression clones through site-specific recombination called LR reaction. This reaction allows construction of respective PCR-fragments in a definite order. However, after LR reaction, DNA sequences coding KGGRADPAFLYKVE, which originates from the sequence of recombination site, remain between center-clone-derived sequence and 3′-clone-derived sequence. All the expression clones are driven by an SV40 enhancer promoter sequence of the 5′ entry clone and have an SV40 poly A signal sequence at the 3′ region derived from pGL4.13 (Promega). The PCR-amplified amino (N)-terminal part, 1−1245 bases, of the luciferase (lucN) sequence (1 corresponding to A at the translational initiation site methionine codon ATG) and the carboxyl (C)-terminal part, 1246−1650 bases, of the luciferase (lucC) sequence derived from pGL4.13, and a β-actin protein coding sequence (Genbank: X03672) amplified from mouse cDNA were used for the construction of the split luciferase probe expression clones. The protein coding sequences of the expression clones nos. 1, 2, 3, and 4 are actin-KGGRADPAFLYKVE-lucN, actin-KGGRADPAFLYKVE-lucC, lucN-KGGRADPAFLYKVE-actin, and lucC-KGGRADPAFLYKVE-actin, respectively (Figure 1B). The linker sequence was further modified by the inverse PCR method[21] using a KOD plus mutagenesis kit (Toyobo). The protein coding sequences of the expression clones nos. 5, 6, 7, 8, 9, and 10 are lucN-GGGGSGGGGSKGGRADPAFLYKVE-actin, lucC-GGGGSGGGGSKGGRADPAFLYKVE-actin, lucN-actin, lucC-actin, lucN-GGGGSGGGGSGGGGS-actin, and lucC-GGGGSGGGGSGGGGS-actin, respectively (Figure 1B).

The MultiSite Gateway system was also used to generate a Cofilin-myc expression clone. A Cofilin (Genbank: BC058726) ORF and a Myc-Tag sequence (EQKLISEEDL) were amplified by PCR and inserted into the center and 3′ entry clones, respectively. Both clones were reacted with pDEST R4-R3, and the 5′ entry clone to obtain a Cofilin-KGGRADPAFLYKVE-Myc-expressing clone driven by an SV40 enhancer promoter.

For the GST fusion lucN-actin and lucC-actin protein expression in *Escherichia coli*, lucN-actin (No. 9) and lucC-actin (No. 10) were amplified by PCR using primers with a *Bam*HI site and a *Not*I site at each end. Amplified fragments were digested with *Bam*HI and *Not*I, then subcloned into the *Bam*HI and *Not*I sites of pGEX-6p-1 (GE Healthcare). All the constructs were confirmed by DNA sequencing using ABI3100 (Applied Biosystems).

Cell Culture and DNA Transfection. HEK293T (1.5×10^5 cells/dish or 0.5×10^5 cells/well) cells were cultured in DMEM supplemented with 10% FCS at 37 °C in 5% CO_2 on a 3-cm-diameter dish (Falcon) for UV irradiation and 3-(4,5-dimethyl-2-thizolyl)-2,5-diphenyl-2*H*-tetrazolium bromide (MTT) assay, and on a glass base dish (Iwaki) for R-P staining. HEK293T cells were transiently transfected using Lipofectamine 2000 (Invitrogen) in accordance with the manufacturer's instructions. Two microgram aliquots of each plasmid were used for cotransfection. When a 24-well culture plate was used for transfection, 4-fold smaller amounts of the reagent and DNA were used. Photon intensity emitted from cells was measured 48 h after transfection.

Cell Viability and Caspase-3 Assays. Cell viability was determined by MTT assay in accordance with the manual attached to the MTT cell viability assay kit (Biotium Inc.). After incubation with the tetrazolium salt MTT (1 mg/mL) for 2 h at room temperature, the harvested cells were solubilized with 1 mL of dimethyl sulfoxide. We measured the absorbance at wavelengths of 570 and 630 nm using a spectrophotometer (Gene Quant 1300, GE Healthcare). The sample signal intensity was obtained by subtraction of OD at 630 nm from OD at 570 nm and indicated as a percentage of the control value. To determine caspase-3 activity, we employed the Caspase 3&7 FLICA kit (ImmunoChemistry Technologies). The cellular substrate FAM-DEVD-FMK was added to the culture medium of the UV-irradiated cells. Fluorescence signals were detected by confocal microscopy (TCS-SP5, Leica).

Western Blotting. Cells were harvested and lysed using M-PER solution (Thermo Scientific). Proteins separated by SDS-PAGE were electrically transferred onto a PVDF membrane (GE Healthcare). The membrane was incubated with an anti-actin primary antibody (1:1000, Santa Cruz) or a polyclonal antiluciferase antibody (1:1000 Promega) in the Can Get Signal solution (Toyobo) at 4 °C overnight. The membrane was reacted with a secondary HRP-conjugated antibody (1:2000, Bio Rad) and visualized using an ECL plus Western blotting reagent (GE Healthcare). Chemiluminescence signals were detected using the LAS-1000 plus system (Fujifilm).

In Vitro Actin Polymerization Assay. Fifty micrograms of pyrene-conjugated actin[22] (Cytoskeleton) with or without probe proteins (1 μg each) was suspended in 2 mL of general actin buffer (5 mM Tris-HCl (pH 8.0), 0.2 mM $CaCl_2$, 0.2 mM ATP, 0.5 mM DTT) and centrifuged at 15 000 *g* for 30 min to remove residual F-actin. To polymerize actin, 1/10 vol of 10× polymerization buffer (500 mM KCl, 20 mM $MgCl_2$, 10 mM ATP) was added. Fluorescence signal intensity was measured every 5 min using a F-4500 spectrophotometer (Hitachi) at an excitation wavelength of 360 ± 10 nm and an emission wavelength of 405 ± 10 nm.

F/G Actin Separation of Cell Lysate by Ultracentrifugation. A G-actin/F-actin *in vivo* assay kit (Cytoskeleton) was used to separate F- and G-actin from the HEK293T lysate. HEK293T cells were lysed in the cell lysis and F-actin stabilization buffer that was provided in the kit. The cell lysate was centrifuged at 100 000 *g* for 1 h at room temperature. The pellet and supernatant were collected as the F-actin-and G-actin-containing fractions, respectively.

Expression of GST-Fusion Probe Proteins in *E. coli*. *E. coli* BL21 (DE3) was transformed by pGEX-6p-1-derived plasmids that encoded GST-lucN-actin and GST-lucC-actin. *E. coli* cells were homogenized by ultrasonication in 1% NP-40 in PBS (pH 7.4). Fusion proteins were purified by binding to glutathione-Sepharose 4B (GE Healthcare). Then, the bound fusion proteins were cleaved with PreScission Protease (GE Healthcare) to obtain lucN-actin and lucC-actin.

Immunoprecipitation Assay. Cofilin-myc and one of the probe proteins (lucN-actin or lucC-actin) were expressed in HEK293T cells. The cells were harvested in PBS, homogenized using a polytron homogenizer (Kinematica), and centrifuged at 2000 *g* for 5 min to remove debris. The protein solution was incubated with 1 μg of an antimyc antibody (Santa Cruz) or 5 μg of an antiluciferase antibody (Promega) bound to 25 μL of protein-G Sepharose (GE Healthcare) for 3 h at 4 °C. Then, the mixtures were washed 5 times, and the precipitates were analyzed by Western blotting using the antimyc (1:1000) and antiluciferase (1:1000) antibodies.

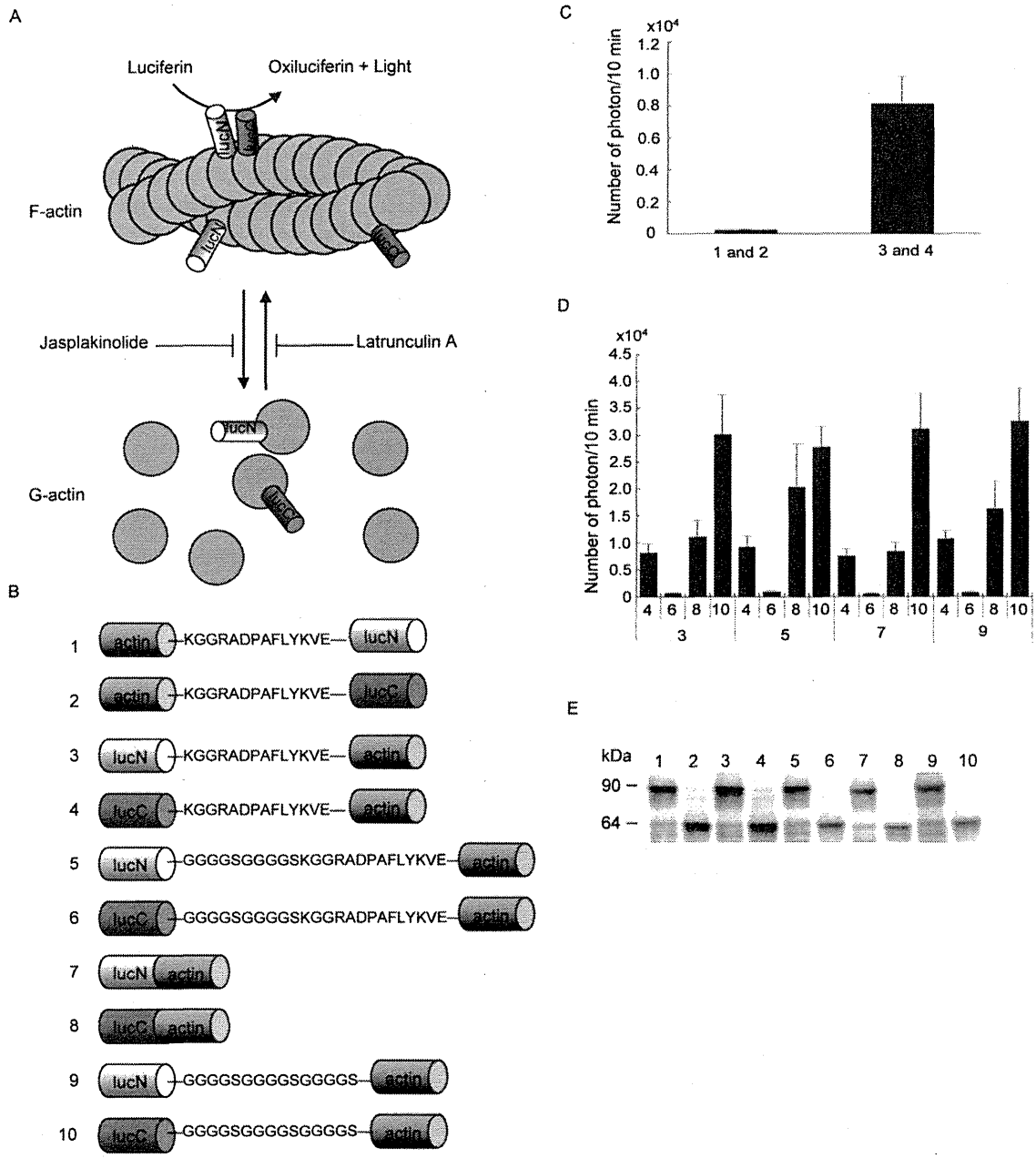

Figure 1. Development of probe proteins to measure actin polymerization. (A) Schema of measurement of level of F-actin based on bioluminescence intensity. LucN and lucC derived from firefly luciferase are fused with actin. Each probe protein is incorporated in the endogenous actin filament. When the lucN and lucC locate close to each other, they recover their luciferase activity and emit light. Jasplakinolide and latrunculin A are the agents that stabilize and inhibit actin polymerization, respectively. (B) Schematic structures of the actin probe proteins encoded by the expression clones nos. 1 to 10. LucN and lucC represent N-terminal and C-terminal split segments of the firefly luciferase, respectively. Amino acid sequences of the linker are indicated as single letters. (C) Combinations of expression clones nos. 1 and 2 and nos. 3 and 4 were expressed in HEK293T and the emitted photons were counted for 10 min using an image intensifier/CCD camera. (D) The numbers of photons emitted from all the combinations of odd and even numbers of clone shown in B except clones nos. 1 and 2 were measured. The numbers on the horizontal axis represent the combinations of probe proteins. All the data are presented as mean ± SEM $n = 4$. (E) The amount of each expressed probe protein was analyzed by Western blotting.

Measuring Photon Intensity Emitted from Cultured Cells. We used an Aequoria-2D/C8600 system (Hamamatsu Photonics) for photon counting. *Wasabi* software (U9304−02) was used for data acquisition and analysis. Cultured cells were taken out from a CO_2 incubator. The culture medium was changed to L15 medium containing 0.5 mM luciferin EF (Promega). The culture plate was placed in a dark box for 30 min. Then, the number of photons emitted from one culture dish well was measured using a charge coupled device (CCD) camera with an image intensifier attached to the top of the dark box. Photon intensity was measured every 5 min continuously for 12 h after UV irradiation or latrunculin A treatments and shown in Figure 4D,E. The numbers of emitted photon from wells were normalized to those from nontreated wells (control) and were plotted as relative intensity.

Cytochemical Staining and Image Acquisition. HEK293T cells were fixed with 4% paraformaldehyde in PBS. Cells were

incubated with 0.14 μM rhodamine-phalloidin (R-P)/PBS for 1 h at room temperature and washed with PBS. Hoechst staining was carried out in accordance with the manual of Caspase 3&7 FLICA kit (ImmunoChemistry Technologies). Fluorescence and bright field images were acquired using a laser confocal microscopy system (TCS-SP5, Leica) with a 63× Plan-Apochromat 1.4 NA lens (Leica) with immersion oil (Type F, Leica) at room temperature. Images were acquired using data acquisition/analysis software of the microscopy system (Leica application suite). No additional software adjustments were performed on images after acquisition. For the R-P signal quantification, the fluorescence intensity of eight randomly taken images using a 20× Plan-Apochromat 0.7 NA lens (Leica) was quantified using the Leica application suite. The intensity of the rhodamine signal was divided by that of the Hoechst staining signal of the same field. Calculated values are represented as a percentage of the control.

UV Irradiation. UV irradiation (at 254 nm, 9.6 kJ/m^2) was performed using a UV cross-linker (Spectrolinker XL-1000, Spectronics). HEK293T cells cultured in 3-cm-diameter dishes were taken out from a CO_2 incubator. The medium was changed to 2 mL of L15 medium (Invitrogen). The cells were irradiated with UV without removing the medium. After the irradiation, the cells were incubated at room temperature for 18 h.

Statistical Analysis. Data are presented as mean ± standard error of the mean (SEM). In the MTT assay, two-tailed Student's *t* test was used to determine statistical significance.

■ RESULTS

Development of Bioluminescence Probes for Long-Term Monitoring of Polymerization of Actin in Living Cells. We developed a novel method to measure the actin polymerization in living cells. The schema to measure the level of F-actin using split luciferase in living cells is shown in Figure 1A. The lucN-actin and lucC-actin fusion proteins are expressed in the cells and are incorporated in the actin filament randomly. When some of the lucN-actin and lucC-actin fusion proteins locate close to each other, they recover their enzymatic activity to emit light. Consequently, the intensity of photon emission is considered to depend on the level of F-actin. We screened the brightest pair of probe proteins. On the basis of the reported optimized cleavage site of firefly luciferase,[14,23] we constructed various luc-actin fusion probe proteins (Figure 1B). Combinations of expression clones nos. 1 and 2 and nos. 3 and 4 were expressed in HEK293T, and the emitted photons were counted for 10 min using the image intensifier/CCD camera. We found that the number of photons emitted from combination of nos. 3 and 4 was about 40 times larger than that of the combination of nos. 1 and 2 (Figure 1C). This result indicated that the N-terminal location of the luc fragment and the C-terminal location of actin are important for emission efficiency. Next, we tested all the combinations of odd and even numbers of expression clones nos. 3−10 (Figure 1B) to determine the brightest probe proteins. We found that the combination of the probe proteins nos. 9 and 10, which contained the flexible linker $(GGGGS)_3$,[24] showed the largest average photon count (Figure 1D) and decided to use this combination in the experiments reported here. To examine whether there were differences in expression level among probe proteins, lucN-actin (~87 kDa) and lucC-actin (~57 kDa) were analyzed by Western blotting using antiluciferase antibody. The difference in expression level of each probe protein was much smaller than the difference in light intensity seen in Figure 1C,D (Figure 1E). We used probes no. 9 (lucN-actin) and 10 (lucC-actin) in the following study.

Characterization of Developed Probe Proteins. To confirm the expression of probe proteins in living cells, lysates from HEK293T expressing probe proteins were analyzed by Western blotting using antiactin antibody. By comparing the intensities of the bands representing lucN-actin (87 kDa), lucC-actin (57 kDa), and endogenous actin (42 kDa), we found that the expression levels of probe ptoteins were less than 5% of endogenous actin (Figure 2A). Next, we determined whether incorporation of probe proteins in F-actin affected the kinetics of actin polymerization *in vitro*. Pyrene-conjugated actin and *E. coli* expressed probe proteins at a molar ratio of 25:1 were mixed in general actin buffer. Then, the polymerization buffer was added to start actin polymerization. The intensity of the fluorescence was measured for 90 min. We observed that the increasing ratio of fluorescence intensity was not changed by the existence of the probe proteins (Figure 2B). Subsequently, the samples used in the reaction were centrifuged to collect the F-actin fraction and analyzed by Western blotting. We detected bands corresponding to lucN-actin and lucC-actin for the sample that was treated with polymerization buffer (probes + P buffer) but not for the sample with general actin buffer alone (probes). This result indicates that incorporation of the probe proteins in F-actin did not affect the kinetics of actin polymerization in vitro (Figure 2C). Next, we confirmed whether the probe proteins were incorporated in F-actin in living cells. To separate F-actin and G-actin, HEK293T cells expressing probe proteins were harvested and ultracentrifuged.[25] The F-actin fraction in the pellet and the G-actin fraction in the supernatant were analyzed by Western blotting using the antiactin and antiluciferase antibodies, and we found that both lucN-actin and lucC-actin probe proteins were contained in each fraction. The ratio of probe proteins in the G-actin fraction to the F-actin fraction was similar to that of endogenous actin (Figure 2D). Then, we examined whether probe proteins could bind to one of the actin-binding proteins. Cofilin,[26] a well-defined actin-binding protein, was fused with the myc-tag sequence and expressed with probe proteins in HEK293T cells. The lysates from HEK293T cells were analyzed by co-immunoprecipitation using antimyc or antiluciferase antibodies. We found that probe proteins and cofilin-myc were contained in precipitated fractions with anti-myc and antiluciferase antibodies, respectively (Figure 2E). These results demonstrated that probe proteins associated with cofilin in the living cells. Finally, we tested whether the probes affect cell proliferation rate. HEK293T cells were transfected with probe proteins or wild-type luciferase (Luc). We did not find any difference in the intensity of MTT signals between the probe proteins- or Luc-expressing cells and the cells treated with lipofectamine alone (Figure 2F). Since light emission levels by luciferase−luciferin reaction and actin polymerization are both ATP-dependent, we tested whether luciferase activity affected the normal actin polymerization. HEK293T cells expressing probe proteins are treated with luciferin for 12 h, and then F- and G-actin fractions were separated. The ratio of F- and G-actin was similar to the control cells that were not treated with luciferin (Figure 2G). Thus, it is considered that normal actin polymerization is not affected by ATP consumption by probe proteins.

Developed Probe Proteins Can Measure the Level of F-Actin in Living Cells. Using the developed probe proteins, we examined whether the intensity of photons emitted by the

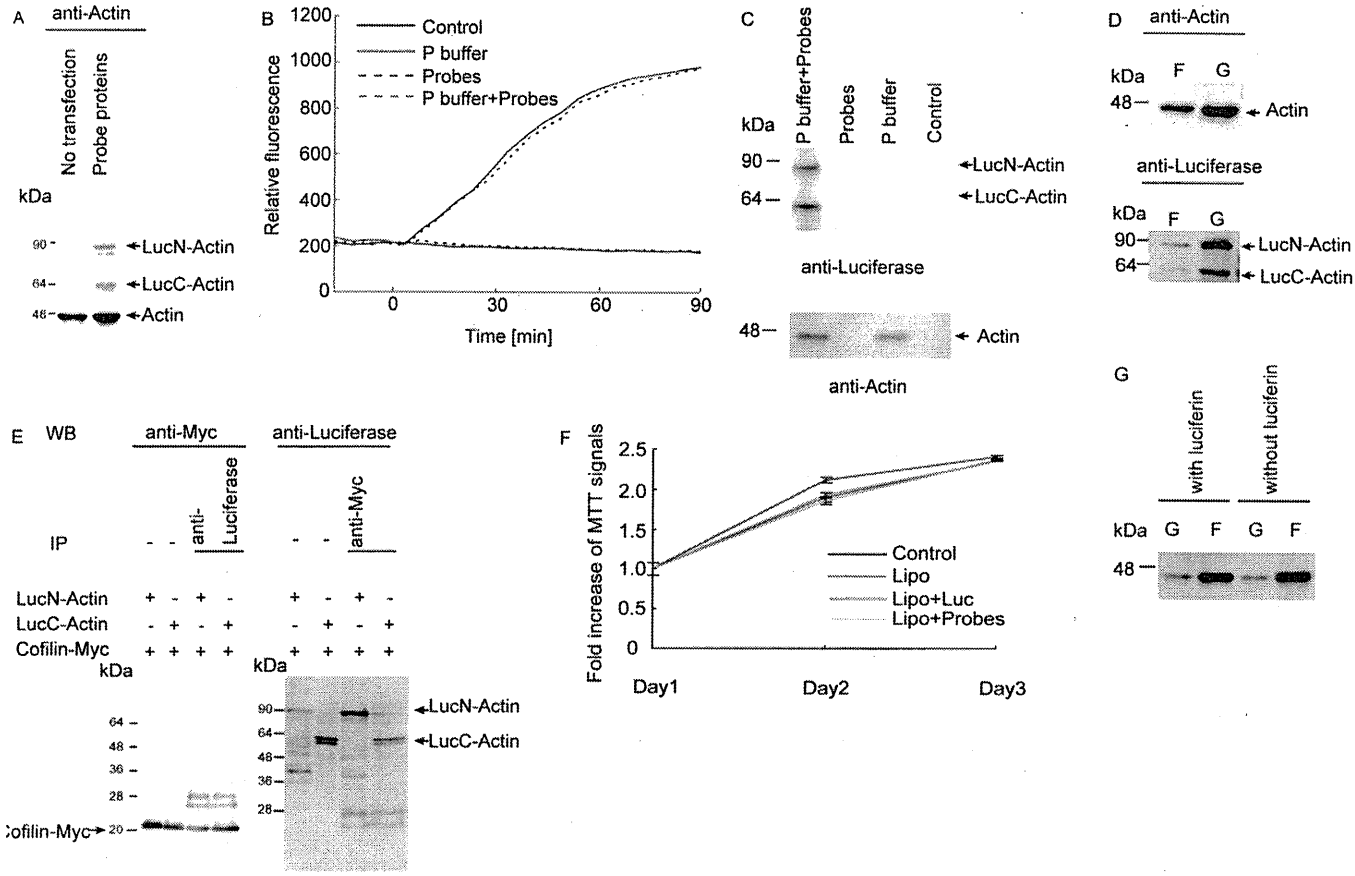

Figure 2. Characterization of probe proteins in vitro and in vivo. (A) Western blotting analysis of endogenous actin and probe proteins. HEK293T cells expressing probe proteins were analyzed by Western blotting using the antiactin antibody. The contrast of the image was adjusted to visualize the luc-actin fusion proteins. (B) Change in fluorescence intensity of pyrene-conjugated actin with probe proteins. Pyrene-actin with (dotted line) or without (solid line) probe proteins was treated with (red line) or without (black line) polymerization (P) buffer, then fluorescence intensity was measured every 5 min for 90 min. (C) Coprecipitation of probe proteins and pyrene-conjugated actin. After the fluorescence observation shown in B, each sample was centrifuged to precipitate F-actin. The pallet was analyzed by Western blotting using the antiluc antibody (upper panel). Then, antiluc antibody was stripped and the membrane was reacted with the antiactin antibody (lower panel). (D) Incorporation of probe proteins in F-actin in cells. HEK293T cells expressing probe proteins were harvested and ultracentrifuged to obtain F-actin in the pellet and G-actin in the supernatant fraction. The pellet was resuspended to the same volume as the supernatant fraction and analyzed by Western blotting. (E) Binding of probe proteins to an actin binding protein cofilin. Cofilin-myc and probe proteins were expressed in HEK293T cells and subjected to immunoprecipitation assay using the antimyc and antiluc antibodies. Total proteins from HEK293T cells expressing both cofilin-myc and one of the probe proteins were incubated with the antiluc (left panel) and antimyc (right panel) antibodies bound to protein-G Sepharose. The immunoprecipitates were analyzed by Western blotting (right two lanes of each panel). The lysate (1%) of transfected cells was directly analyzed by Western blotting as controls (left two lanes of each panel). (F) HEK293T cells were transfected with the plasmids that encoded wild-type luciferase (Luc) or probe proteins (Probes), the combination of nos. 9 and 10 (Figure 1B), using lipofectoamine 2000 (Lipo) on day 1. In the control, no plasmid or lipofectamine 2000 was added (Control). Cell viability was measured by the MTT method on days 1−3. Data are presented as mean ± SEM, $n = 4$. (G) F- and G-actin fractions from the cells expressing probe proteins in the presence (left) or absence (right) of luciferin were analyzed by Western blotting. In each Western blot, the locations of molecular weight markers (kDa) are shown on the left. Arrows indicate the locations of the bands corresponding to lucN-actin, lucC-actin, endogenous actin, and cofilin-myc.

probe proteins precisely reflected the level of F-actin in the cells. We added various concentrations of latrunculin A, which disrupts the actin filament by binding to G-actin,[27] to the culture medium of HEK293T expressing the probe proteins. After 3 h incubation with latrunculin A, luciferin was added and photon intensity was measured using the image intensifier/CCD camera in a dark box. We did not set any threshold to cut off the background noise. Depending on the latrunculin A concentration, photon intensity decreased (Figure 3A). At the highest concentration (50 μM) of latrunculin A, the photon emission was diminished almost completely. In the control experiment, Luc was expressed in the HEK293T cells and treated in the same manner as in Figure 3A. We observed no reduction in photon intensity following the treatment (Figure 3B). These results demonstrated that latrunculin A did not affect the activity of wild-type luciferase. Next, we evaluated the measurement of F-actin level in the cells using a conventional F-actin staining method. Cells were fixed after latrunculin A treatment and stained with R-P. Fluorescence microscopy analysis showed a dose-responsive decrease in fluorescence signal intensity, which represented the level of F-actin, accompanied with rounding of the cell shape (Figure 3C). The fluorescence signal intensity decreased with increasing concentration of latrunculin A (Figure 3D). However, at the highest concentration of latrunculin A (50 μM), the fluorescence intensity was about 30% of that of control cells and did not completely disappear (Figure 3D). Furthermore, the effect of an F-actin-

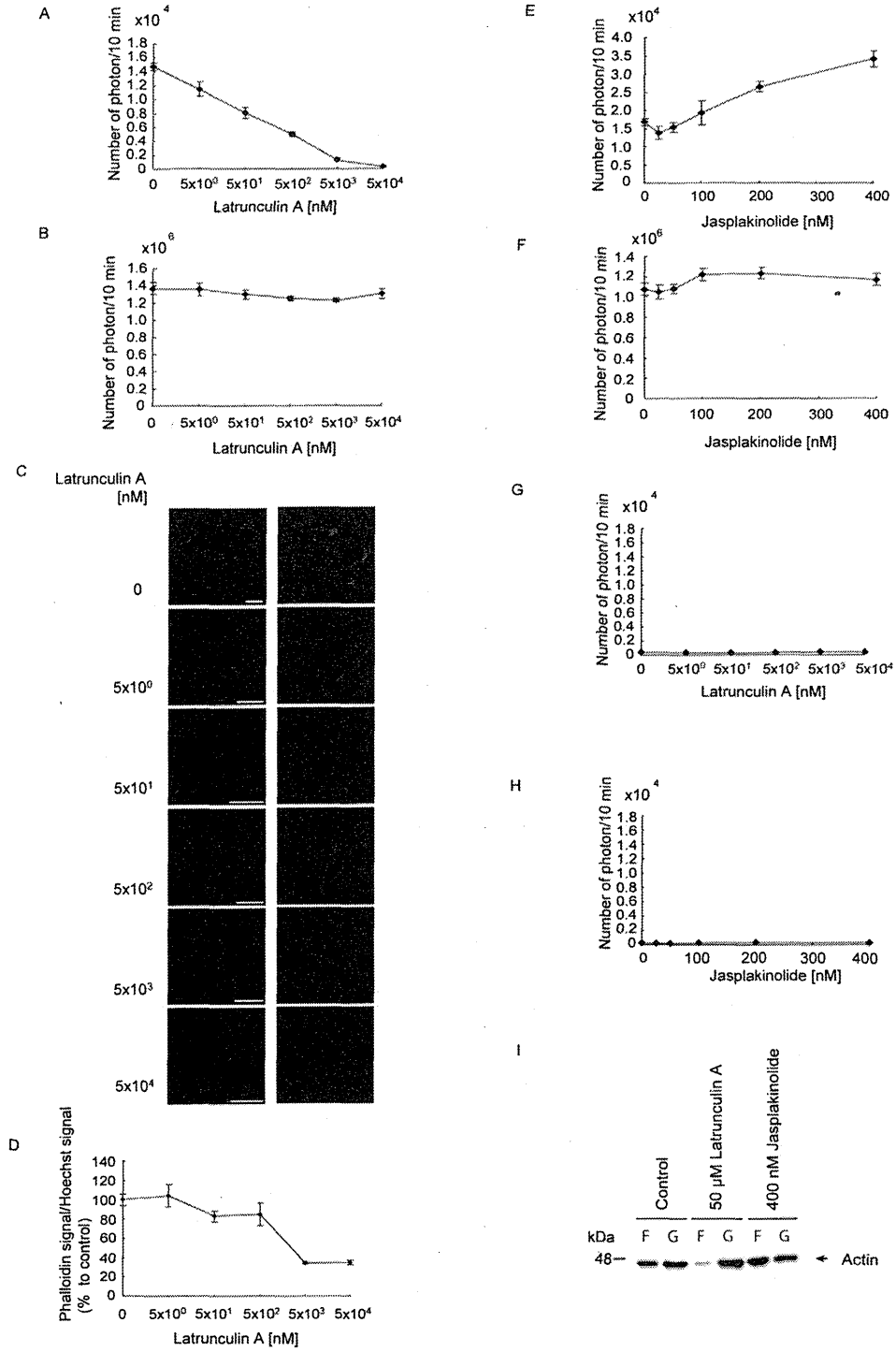

Figure 3. Effect of latrunculin A treatment on photon emission from F-actin probe proteins. (A) Concentration-dependent inhibition of photon emission from F-actin probe proteins by latrunculin A. The combination of probe proteins nos. 9 and 10 (Figure 1B) was expressed in HEK293T cells. Cells were treated with the indicated concentration of latrunculin A for 3 h. The intensity of photon emission in a period of 10 min from each culture well was measured. (B) Effect of latrunculin A on wild-type luciferase. The intensity of photon emission from the culture well expressing wild-type luciferase was measured as in (A). (C) Effects of latrunculin A on rhodamine-phalloidin (R-P) staining of HEK293T cells. Cells were treated with latrunculin A for 3 h and fixed. Red fluorescence represents F-actin. Fluorescence and bright field images were obtained by confocal microscopy. Bars indicate 10 μm. (D) Effects of latrunculin A on R-P staining of F-actin. R-P fluorescence signal intensity was normalized with Hoechst signal intensity. The values are expressed as a percentage of the control experiments without latrunculin A treatment. (E) Concentration-dependent increase in the intensity of photon emission from F-actin probe proteins after treatment with jasplakinolide. (F) Effect of jasplakinolide on wild-type luciferase. Photon emission was measured in the same manner as in (E). (G) Effects of latrunculin A on photon emissions from the cells expressing lucN and lucC. (H) Effects of jasplakinolide on photon emissions from the cells expressing lucN and lucC. (I) The amounts of F- and G- actin were analyzed by Western blotting after latrunculin A and jasplakinolide treatment. All the data are presented as mean ± SEM, $n = 4$ in (A, B, E, F, G, and H). $n = 8$ in (D).

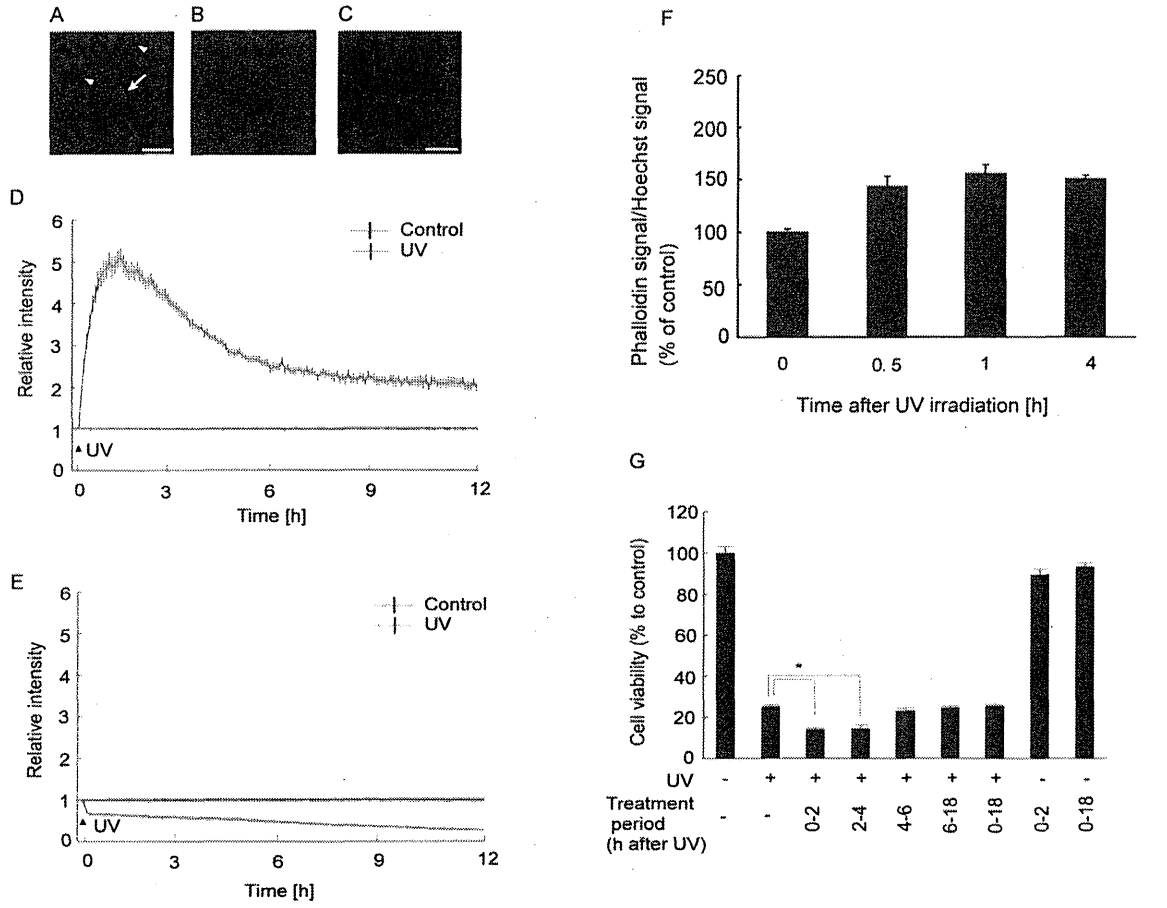

Figure 4. Effects of latrunculin A treatment on UV-induced apoptosis of HEK293T cells. (A) Cytochemistry of UV-irradiated cells stained with Hoechst (blue) 8 h after UV irradiation. The arrow indicates a cell with a condensed nucleus. Arrowheads indicate nuclear-membrane-localized chromatin stained with Hoechst. (B) Cells shown in A stained with caspase-3 activity indicator (green). (C) Non-UV-irradiated cells stained with Hoechst (blue). Bars indicate 10 μm in (A) and (C). (D) Time course of relative intensity of photon emission from F-actin probe proteins after UV irradiation (arrowhead). The red line represents the data from UV-irradiated cells. The black line represents that from the non-UV-irradiated control. (E) Time course of relative intensity of photon emission from cells expressing wild-type luciferase after UV irradiation. (F) Effects of UV on R-P staining of F-actin. The R-P fluorescence signals were normalized with Hoechst signals. The values are expressed as a percentage of the signal at time 0. (G) Effects of UV irradiation and latrunculin A treatment on cell viability assayed by the MTT method. Cells with and without UV irradiation were treated with or without 500 nM latrunculin A for indicated periods. Eighteen hours after UV irradiation, cell viability was measured. Cell viability is represented as a percentage of the viability of the control cells without UV irradiation and latrunculin A treatment. All the data are presented as mean ± SEM, $n = 4$, in (D,E,G). $n = 12$ in (F). * $p < 0.05$.

stabilizing reagent, jasplakinolide,[28] on photon emission from the probe proteins was tested. When jasplakinolide of more than 200 nM was added to the cells expressing the probe proteins, the cells emitted a significantly stronger light than when lower concentrations (<100 nM) were added (Figure 3E). We also tested a higher concentration (>400 nM) of jasplakinolide on the transfected cells and observed the tendency to emit a stronger light, but in those cases, the cells were often detached from the culture dishes (data not shown). We found that the photon emission of wild-type luciferase was not affected by jasplakinolide treatment (Figure 3F). The effects of jasplakinolide treatment on photon emission also support the idea that the photon intensity emitted from probe proteins quantitatively reflects the level of F-actin. Analysis of the effects of jasplakinolide on R-P staining of cells was not carried out because the binding sites of phalloidin and jasplakinolide are the same.[28] In order to confirm that lucN and lucC without actin fusing them do not interact each other, we measured the light intensity from the cells expressing lucN and lucC. The light intensity was much lower than the cells expressing lucN-actin and lucC-actin and did not react to latrunculin A and jasplakinolide (Figure 3G,H) as reported before.[29] To test whether latrunculin A and jasplakinolide change the amount of F-actin, HEK293T cells treated with the compounds were harvested, and F- and G- fractions were separated by centrifuge. The amount of F-actin was markedly reduced by latrunculin A and increased by jasplakinolide (Figure 3I). These changes of F-actin level are similar to the changes of light intensities seen in Figure 3A and E, supporting the functionality of the probe proteins.

Measurement of Actin Polymerization in HEK293T after UV Irradiation. We next applied these probe proteins to analyze the state of actin polymerization during apoptosis. First, we tried to characterize the HEK293T cell death induced by UV irradiation as a model. Fluorescence microscopy revealed that UV-irradiated cells exhibited nuclear condensation and chromatin localization at the nuclear membrane, as shown by Hoechst staining (Figure 4A), compared with the control cells (Figure 4C). In the cells that exhibited nuclear condensation, caspase-3 activation was observed (Figure 4B). These cells were

frequently detached from the culture dish (data not shown). Since these features were reported in lower-intensity UV- and cadmium-induced HEK293 apoptosis,[30,31] we assumed that the UV irradiation induced the apoptotic cell death. Then, we monitored the change in F-actin level after UV irradiation in real time and in living cells. Cells expressing the probe proteins were irradiated with UV, in the same manner as shown in Figure 4A, and photon emission intensity was measured continuously for 12 h after irradiation. We found that the relative photon intensity transiently increased after irradiation and gradually decreased after 2 h (Figure 4D). In the control experiment, Luc-expressing cells showed a decrease rather than an increase in photon emission intensity, which might be due to the toxic effect of UV irradiation (Figure 4E). Using conventional R-P staining, a transient increase of F-actin after UV irradiation was also detected, but the increase in signal was lower than that of our probes (Figure 4F). Considering the result of Figure 4D, we predicted that transient upregulation of F-actin in early phase (0−4 h) of apoptosis progression would be a protective reaction of the cell as reported in different cell lines.[16−18] To test this prediction, we determined the effects of latrunculin A on UV-induced HEK293T cell death. After the UV irradiation, 500 nM latrunculin A was added to the cells. Cell death was measured 18 h after irradiation by the MTT method. We found that the treatment with latrunculin A for 0−2 and 2−4 h after irradiation significantly enhanced UV-induced cell death (Figure 4G). In contrast, latrunculin A treatment 4 h after UV irradiation did not change the MTT signal intensity. Since latrunculin A treatment without UV did not induce significant cell death (Figure 4G), these results indicate that latrunculin A treatment accelerates UV-induced cell death only in the early period (0−4 h) after the irradiation. The period during which F-actin upregulation peaked (1−2 h after UV irradiation) (Figure 4D) overlapped with the period during which latrunculin A (500 nM) effectively enhanced the UV-induced cell death (0−2 h after UV irradiation) (Figure. 4G), suggesting a protective role of upregulated F-actin against apoptosis.

■ DISCUSSION

Characterization of the Probe Proteins We Developed. We successfully developed and improved the photon emission intensity of probe proteins to monitor actin polymerization (Figure 1). Expression of the probe proteins did not have any effect on HEK293T cell proliferation and actin polymerization ratio in vitro (Figure 2B,F). The probe proteins were incorporated in F-actin in vitro and in vivo (Figure 2C,D), and photon emission intensity decreased with increasing latrunculin A concentration (Figure 3A). The changes in photon emission of probe proteins induced by UV irradiation and latrunculin A treatments were consistent with those of R-P staining (Figure 3C,D). Above all, we conclude that our probe proteins can be used to precisely monitor actin polymerization in living cells. In previous studies, phalloidin has served as a useful tool to stain F-actin;[8] however, this reagent cannot be used in living cells because it requires cell fixation. The fluorescent GFP-actin protein[9] and lifeact[10] have been utilized to image the subcellular distribution of F-actin in living cells. However, these fusion proteins emit fluorescence even if they are monomers, and so are not suitable for quantification of the level of F-actin. Recently, the FRET technique has been employed to monitor F-actin,[11] although the FRET signal intensity is not in proportion to the level of F-actin.[12] These methods based on fluorescence observation have limits of autofluorescence noise and phototoxicity.[32] On the other hand, our probe proteins have little noise and no phototoxicity since no excitation light is required. These advantages enable us to carry out long-term quantitative measurement of F-actin in living cells (Figure 4). Since actin is a universal protein among all eukaryotic cells, and many cellular events are related to F-actin organization, our novel probe proteins can be applied to the analysis of a wide variety of phenomena involving actin polymerization in cells.

The increasing ratio of photon emission from probe proteins (Figure 4D) was higher than that of R-P signals (Figure 4F) in response to UV irradiation. Even if a high concentration of latrunculin A (50 μM) was added, we detected fluorescent signals from cells (Figure 3D), whereas the photon intensity from our probe proteins was diminished almost completely (Figure 3A). Thus, the main reason for this difference might be considered to be that the R-P signals contain about 40% of autofluorescence noise. In addition, another possibility that some F-actin was detected by R-P method and not by our method may explain the remained R-P fluorescence in Figure 3D. This point should be elucidated in the future.

The expression levels of our probe proteins are lower than that of GFP-actin.[33] Since GFP is known to have high stability,[34] it is possible that luc-actin fusion proteins are easier to be degraded than GFP-actin protein. This is a disadvantage because the degradation of probes reduces signal intensity. On the other hand, lower stability of our probe proteins may be an advantage, as they do not affect normal cell activities such as proliferation (Figure 2F).

Transient Increase in F-Actin Level Is Likely a Defensive Reaction of Cells. Some reports indicated F-actin disruption induced the apoptosis, and other reports showed enhancement of apoptosis by treatment with F-actin disruptive agent after apoptosis-inducing stimulation.[16−18] Thus, it is suggested F-actin has a protective role for the cells. However, the precise time course of actin polymerization during cell death has not been elucidated. Using our probe proteins, we succeeded in real-time monitoring of the actin polymerization in living cells after apoptosis induction and found that F-actin level was upregulated transiently after UV irradiation (Figure 4D). Furthermore, F-actin disruption with latrunculin A in the early period (0−2, 2−4 h after UV irradiation) enhanced the cell death, whereas later treatment (4−6, 6−18 h after UV irradiation) did not (Figure 4G). These results indicate that actin polymerization occurs in the early phase of apoptosis and support the hypothesis of protective role of actin polymerization against the cell death. In UV-induced apoptosis, several pathways are reported;[35] further study combined with pharmacological methods will reveal the mechanism of protective effect of actin polymerization on cell death.

■ AUTHOR INFORMATION

Corresponding Author

*Hisashi Mori, Ph.D., University of Toyama, 2630 Sugitani, Toyama 930-0194, Japan. Tel: +81-76-434-7230. Fax: +81-76-434-5015. E-mail: hmori@med.u-toyama.ac.jp.

■ ACKNOWLEDGMENT

This work was supported by PRESTO of the Japan Science and Technology Corporation (JST, No. 2602) and the Japan

Society for the Promotion of Science (JSPS, No. 2070331). The authors declare no competing financial interests.

REFERENCES

(1) Bailly, M., and Condeelis, J. (2002) Cell motility: insights from the backstage. *Nat. Cell Biol. 4*, E292–4.

(2) Mitchison, T. J., and Cramer, L. P. (1996) Actin-based cell motility and cell locomotion. *Cell 84*, 371–9.

(3) Sahai, E. (2005) Mechanisms of cancer cell invasion. *Curr. Opin. Genet. Dev. 15*, 87–96.

(4) Fukazawa, Y., Saitoh, Y., Ozawa, F., Ohta, Y., Mizuno, K., and Inokuchi, K. (2003) Hippocampal LTP is accompanied by enhanced F-actin content within the dendritic spine that is essential for late LTP maintenance in vivo. *Neuron 38*, 447–60.

(5) Matsuzaki, M., Honkura, N., Ellis-Davies, G. C., and Kasai, H. (2004) Structural basis of long-term potentiation in single dendritic spines. *Nature 429*, 761–6.

(6) Franklin-Tong, V. E., and Gourlay, C. W. (2008) A role for actin in regulating apoptosis/programmed cell death: evidence spanning yeast, plants and animals. *Biochem. J. 413*, 389–404.

(7) Ndozangue-Touriguine, O., Hamelin, J., and Breard, J. (2008) Cytoskeleton and apoptosis. *Biochem. Pharmacol. 76*, 11–8.

(8) Wulf, E., Deboben, A., Bautz, F. A., Faulstich, H., and Wieland, T. (1979) Fluorescent phallotoxin, a tool for the visualization of cellular actin. *Proc. Natl. Acad. Sci. U.S.A. 76*, 4498–502.

(9) Doyle, T., and Botstein, D. (1996) Movement of yeast cortical actin cytoskeleton visualized in vivo. *Proc. Natl. Acad. Sci. U.S.A. 93*, 3886–91.

(10) Riedl, J., Crevenna, A. H., Kessenbrock, K., Yu, J. H., Neukirchen, D., Bista, M., Bradke, F., Jenne, D., Holak, T. A., Werb, Z., Sixt, M., and Wedlich-Soldner, R. (2008) Lifeact: a versatile marker to visualize F-actin. *Nat. Methods 5*, 605–7.

(11) Okamoto, K., and Hayashi, Y. (2006) Visualization of F-actin and G-actin equilibrium using fluorescence resonance energy transfer (FRET) in cultured cells and neurons in slices. *Nat. Protoc. 1*, 911–9.

(12) Takanishi, C. L., Bykova, E. A., Cheng, W., and Zheng, J. (2006) GFP-based FRET analysis in live cells. *Brain Res. 1091*, 132–9.

(13) Ozawa, T., Kaihara, A., Sato, M., Tachihara, K., and Umezawa, Y. (2001) Split luciferase as an optical probe for detecting protein-protein interactions in mammalian cells based on protein splicing. *Anal. Chem. 73*, 2516–21.

(14) Luker, K. E., Smith, M. C., Luker, G. D., Gammon, S. T., Piwnica-Worms, H., and Piwnica-Worms, D. (2004) Kinetics of regulated protein-protein interactions revealed with firefly luciferase complementation imaging in cells and living animals. *Proc. Natl. Acad. Sci. U.S.A. 101*, 12288–93.

(15) Paulmurugan, R., Umezawa, Y., and Gambhir, S. S. (2002) Noninvasive imaging of protein-protein interactions in living subjects by using reporter protein complementation and reconstitution strategies. *Proc. Natl. Acad. Sci. U.S.A. 99*, 15608–13.

(16) Suria, H., Chau, L. A., Negrou, E., Kelvin, D. J., and Madrenas, J. (1999) Cytoskeletal disruption induces T cell apoptosis by a caspase-3 mediated mechanism. *Life Sci. 65*, 2697–707.

(17) Martin, S. S., and Leder, P. (2001) Human MCF10A mammary epithelial cells undergo apoptosis following actin depolymerization that is independent of attachment and rescued by Bcl-2. *Mol. Cell. Biol. 21*, 6529–36.

(18) Celeste Morley, S., Sun, G. P., and Bierer, B. E. (2003) Inhibition of actin polymerization enhances commitment to and execution of apoptosis induced by withdrawal of trophic support. *J. Cell Biochem. 88*, 1066–76.

(19) Hartley, J. L., Temple, G. F., and Brasch, M. A. (2000) DNA cloning using in vitro site-specific recombination. *Genome Res. 10*, 1788–95.

(20) Sasaki, Y., Sone, T., Yoshida, S., Yahata, K., Hotta, J., Chesnut, J. D., Honda, T., and Imamoto, F. (2004) Evidence for high specificity and efficiency of multiple recombination signals in mixed DNA cloning by the Multisite Gateway system. *J. Biotechnol. 107*, 233–43.

(21) Ochman, H., Gerber, A. S., and Hartl, D. L. (1988) Genetic applications of an inverse polymerase chain reaction. *Genetics 120*, 621–3.

(22) Cooper, J. A., Walker, S. B., and Pollard, T. D. (1983) Pyrene actin: documentation of the validity of a sensitive assay for actin polymerization. *J. Muscle Res. Cell Motil. 4*, 253–62.

(23) Kim, S. B., Kanno, A., Ozawa, T., Tao, H., and Umezawa, Y. (2007) Nongenomic activity of ligands in the association of androgen receptor with SRC. *ACS Chem. Biol. 2*, 484–92.

(24) Huston, J. S., Levinson, D., Mudgett-Hunter, M., Tai, M. S., Novotny, J., Margolies, M. N., Ridge, R. J., Bruccoleri, R. E., Haber, E., and Crea, R. et al. (1988) et al. Protein engineering of antibody binding sites: recovery of specific activity in an anti-digoxin single-chain Fv analogue produced in Escherichia coli. *Proc. Natl. Acad. Sci. U.S.A. 85*, 5879–83.

(25) Tu, Y., Wu, S., Shi, X., Chen, K., and Wu, C. (2003) Migfilin and Mig-2 link focal adhesions to filamin and the actin cytoskeleton and function in cell shape modulation. *Cell 113*, 37–47.

(26) Bernstein, B. W., and Bamburg, J. R. ADF/cofilin: a functional node in cell biology. *Trends Cell Biol. 20*, 187-95.

(27) Coue, M., Brenner, S. L., Spector, I., and Korn, E. D. (1987) Inhibition of Actin Polymerization by Latrunculin-A. *Febs Lett. 213*, 316–318.

(28) Bubb, M. R., Senderowicz, A. M., Sausville, E. A., Duncan, K. L., and Korn, E. D. (1994) Jasplakinolide, a cytotoxic natural product, induces actin polymerization and competitively inhibits the binding of phalloidin to F-actin. *J. Biol. Chem. 269*, 14869–71.

(29) Paulmurugan, R., and Gambhir, S. S. (2005) Firefly luciferase enzyme fragment complementation for imaging in cells and living animals. *Anal. Chem. 77*, 1295–302.

(30) Fan, Y., Wu, D., Jin, L., and Yin, Z. (2005) Human glutamyl-cysteine synthetase protects HEK293 cells against UV-induced cell death through inhibition of c-Jun NH2-terminal kinase. *Cell Biol. Int. 29*, 695–702.

(31) Mao, W. P., Ye, J. L., Guan, Z. B., Zhao, J. M., Zhang, C., Zhang, N. N., Jiang, P., and Tian, T. (2007) Cadmium induces apoptosis in human embryonic kidney (HEK) 293 cells by caspase-dependent and -independent pathways acting on mitochondria. *Toxicol. In Vitro 21*, 343–54.

(32) Dixit, R., and Cyr, R. (2003) Cell damage and reactive oxygen species production induced by fluorescence microscopy: effect on mitosis and guidelines for non-invasive fluorescence microscopy. *Plant J. 36*, 280–90.

(33) Westphal, M., Jungbluth, A., Heidecker, M., Muhlbauer, B., Heizer, C., Schwartz, J. M., Marriott, G., and Gerisch, G. (1997) Microfilament dynamics during cell movement and chemotaxis monitored using a GFP-actin fusion protein. *Curr. Biol. 7*, 176–83.

(34) Enoki, S., Saeki, K., Maki, K., and Kuwajima, K. (2004) Acid denaturation and refolding of green fluorescent protein. *Biochemistry 43*, 14238–48.

(35) Kulms, D., and Schwarz, T. (2000) Molecular mechanisms of UV-induced apoptosis. *Photodermatol. Photoimmunol. Photomed. 16*, 195–201.

CORRESPONDENCE

Is D-Cycloserine a Prodrug for D-Serine in the Brain?

To the Editor:

D-cycloserine (DCS), (4*R*)-4-amino-1,2-oxazolidin-3-one, is a partial agonist at the strychnine-insensitive glycine modulatory site associated with the *N*-methyl-D-aspartate (NMDA) receptor complex. DCS is also a less efficient ligand of NMDA receptor function than endogenous full agonists, such as glycine and D-serine. At high doses, DCS acts as an antagonist by displacing more efficacious endogenous agonists, but at moderate doses, DCS facilitates glutamatergic neurotransmission via the NMDA receptor. Recent meta-analysis shows that glycine, D-serine, and sarcosine (*N*-methylglycine), an endogenous glycine transporter-1 inhibitor, are more effective than DCS in improving the overall psychopathology in patients with schizophrenia receiving antipsychotic drugs (1). This suggests a relatively narrow therapeutic window for DCS, most likely due to its partial agonist properties.

A meta-analysis of both animals and humans demonstrated that DCS enhances prolonged exposure therapy, a cognitive-behavioral therapy, used in patients with anxiety disorders, such as posttraumatic stress disorder (PTSD), social phobia, panic disorder, and obsessive-compulsive disorder (2), although a recent meta-analysis conducted in humans showed no significant effects of dose timing or dose number on the treatment efficacy of DCS (3). Animal studies have suggested that fear of extinction has been linked to NMDA receptor function in the basolateral amygdala and that DCS can enhance extinction effects (4). When fear extinction takes place during DCS treatment, the usual forms of neuroplasticity are enhanced, along with the recruitment of additional forms of neuroplasticity, to enhance extinction and protect against reinstatement (5). These findings imply that DCS could be an effective therapeutic agent for enhancing exposure-based therapy in anxiety disorders (2,3,5), although further detailed studies are needed.

Here we report that treatment with DCS can increase extracellular levels of D-serine in the brain. An in vivo microdialysis study using free-moving mice showed that extracellular levels of D-serine in the mouse hippocampus were significantly increased after oral (100 mg/kg) or intracerebroventricular (ICV) infusion of DCS (10 mmol/L, 1 μL/min for 30 min; Figure 1). Previously, we reported that extracellular levels of D-serine in the hippocampus of serine racemase (*Srr*) knockout (KO) mice were markedly decreased to approximately 20% of levels in wild-type mice, indicating that serine racemase (SRR) is the major enzyme responsible for D-serine production in the mouse forebrain (6) (Figure 1). Interestingly, oral dosing or ICV infusion of DCS induced a marked increase in extracellular D-serine levels within the hippocampus of *Srr*-KO mice (Figure 1). In contrast, DCS administration did not alter extracellular levels of glycine in this region (data not shown). These findings suggest that SRR does not play a role in the mechanisms that induce increases of D-serine in mouse brains after DCS treatment.

It is well known that DCS is unstable in aqueous solutions, where it is converted into the biologically inactive dimer, 2,5-bis-(aminooxymethyl)-3,6-diketopiperazine (7). Furthermore, DCS can be synthesized from the precursor D-serine. Given that SRR is not required for the production of D-serine in the brain after DCS treatment, D-serine may indeed become available on degradation of DCS because of the inherent instability of DCS in brain extracellular fluids. Interestingly, a pilot study showed that D-serine (30 mg/kg/day) was effective in treating PTSD (8). It is therefore likely that the D-serine produced in the brain after DCS treatment plays at least a partial role in the therapeutic effects of DCS seen in patients with anxiety disorders. Nonetheless, additional study using DCS labeled with isotopes will be needed to confirm this hypothesis.

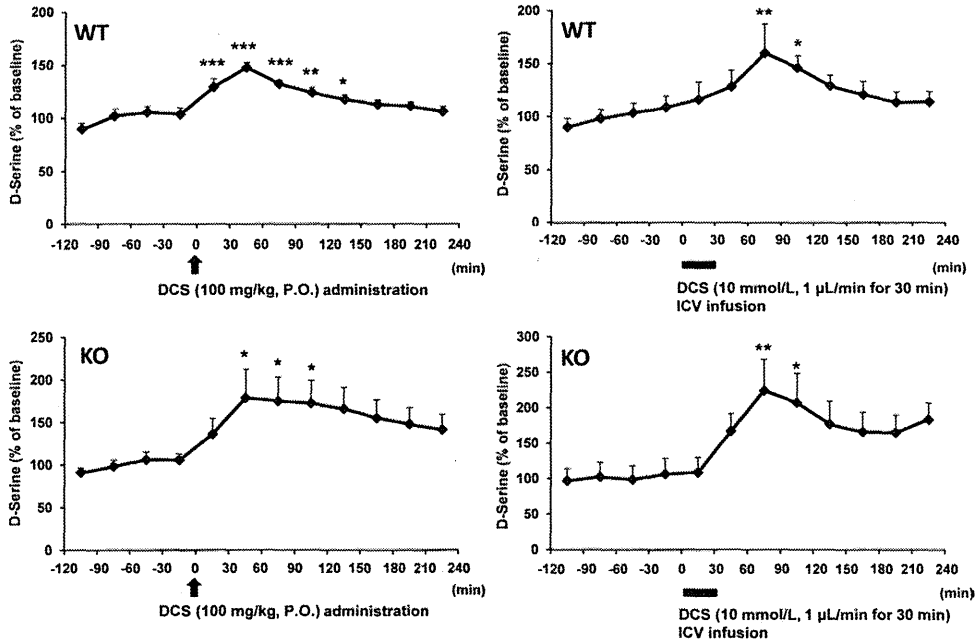

Figure 1. Extracellular D-serine levels in the hippocampus after D-cycloserine (DCS) treatment. Extracellular levels of D-serine in the hippocampus of wild-type (WT) mice and *Srr*-knockout (KO) mice were significantly increased after oral (P.O.; 100 mg/kg) or intracerebroventricular (ICV; 10 mmol/L, 1 μL/min for 30 min) administration of DCS. The average values of baseline in the hippocampus of WT mice and *Srr*-KO mice were .358 ± .015 μmol/L ($n = 12$) and .075 ± .002 μmol/L ($n = 12$), respectively. Data show the mean ± SEM. Data were analyzed using one-way analysis of variance, post hoc Fisher's protected least significant difference to compare individual postinjection time points to collapsed average baselines values (100%). $^*p < .05$, $^{**}p < .01$, $^{***}p < .001$ compared with baseline values.

0006-3223/$36.00

Taking all of this information together, it is reasonable to propose that DCS may act as a prodrug for D-serine in the brain. This idea is based on the greater permeability of DCS into the brain compared with D-serine and the unstable nature of DCS in brain extracellular fluids. This degradation of DCS will result in increased D-serine bioavailability within the brain. However, there is also the possibility that the action of D-serine produced from DCS may in turn be antagonized by DCS, resulting in no significant effects in its treatment efficacy for anxiety disorders (3). The low availability of D-serine due to degradation by D-amino acid oxidase in peripheral organs hampers its use in disease treatment because high levels would be needed to achieve therapeutic doses. Therapeutic levels could be achieved if D-serine were administered with D-amino acid oxidase inhibitors. This combination may well provide a more effective and an alternative therapeutic approach to that of DCS (9,10).

Mao Horio[a]
Hisashi Mori[b]
Kenji Hashimoto[a]*

[a]Division of Clinical Neuroscience, Chiba University Center for Forensic Mental Health, Chiba, Japan, and [b]Department of Molecular Neuroscience, Graduate School of Medicine and Pharmaceutical Sciences, University of Toyama, Toyama, Japan

*Corresponding author E-mail: hashimoto@faculty.chiba-u.jp.

This study was supported by a Grant-in-Aid for Scientific Research (B) (to KH) from Japan Society for the Promotion of Science and a Grant-in-Aid for Scientific Research (to KH) from Ministry of Education, Cultural, Sports, Science and Technology (MEXT), Japan.

The authors report no biomedical financial interests or potential conflicts of interest.

1. Tsai GE, Lin PY (2010): Strategies to enhance *N*-methyl-D-aspartate receptor-mediated neurotransmission in schizophrenia. A critical review and meta-analysis. *Curr Pham Des* 16:522–537.
2. Nordberg MM, Krystal JH, Tolin DF (2008): A meta-analysis of D-cycloserine and the facilitation of fear extinction and exposure therapy. *Biol Psychiatry* 63:1118–1126.
3. Bontempo A, Panza KE, Bloch MH (2012): D-Cycloserine augmentation of behavioral therapy for the treatment of anxiety disorders: A meta-analysis. *J Clin Psychiatry* 73:533–537.
4. Davis M, Ressler K, Rothbaum RO, Richardson R (2006): Effects of D-cycloserine on extinction: Translation from preclinical to clinical work. *Biol Psychiatry* 60:369–375.
5. Krystal LH (2012): Enhancing prolonged exposure therapy for posttraumatic stress disorder with D-cycloserine: Further support for treatments that promote experience-dependent neuroplasticity. *Biol Psychiatry* 71: 932–934.
6. Horio M, Kohno M, Fujita Y, Ishima T, Inoue R, Mori H, *et al.* (2011): Levels of D-serine in the brain and peripheral organs of serine racemase (*Srr*) knock-out mice. *Neurochem Int* 59:853–859.
7. Higy PH, Hodge EB, Young VV, Harned RL, Brewer GA, Philips WF, *et al.* (1955): Structure and reactions of cycloserine. *J Am Chem Soc* 77:2345–2346.
8. Heresco-Levy U, Vass A, Bloch B, Wolosker H, Dumin E, Balan L, *et al.* (2009): Pilot controlled trial of D-serine for the treatment of post-traumatic stress disorder. *Int J Neuropsychopharmacol* 12:1275–1282.
9. Ferraris D, Duvall B, Ko YS, Thomas AG, Rojas C, Majer P, *et al.* (2008) Synthesis and biological evaluation of D-amino acid oxidase inhibitors. *J Med Chem* 51:3357–3359.
10. Hashimoto K, Fujita Y, Horio M, Kunitachi S, Iyo M, Ferraris D, *et al.* (2009): Co-administration of D-amino acid oxidase inhibitor potentiates the efficacy of D-serine on prepulse inhibition deficits after administration of dizocilpine. *Biol Psychiatry* 65:1103–1106.

http://dx.doi.org/10.1016/j.biopsych.2012.07.013

Epilepsy Research (2012) 102, 180–187

journal homepage: www.elsevier.com/locate/epilepsyres

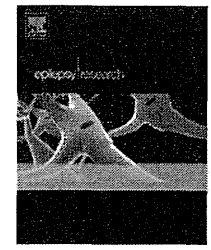

Decreased susceptibility to seizures induced by pentylenetetrazole in serine racemase knockout mice

Tomomi Harai[a,b,1], Ran Inoue[a,1], Yuko Fujita[c], Ayumi Tanaka[a], Mao Horio[c], Kenji Hashimoto[c], Kazuhisa Hongou[b], Toshio Miyawaki[b], Hisashi Mori[a,*]

[a] *Department of Molecular Neuroscience, Graduate School of Medicine and Pharmaceutical Sciences, University of Toyama, Toyama 930-0194, Japan*
[b] *Department of Pediatrics, Graduate School of Medicine and Pharmaceutical Sciences, University of Toyama, Toyama 930-0194, Japan*
[c] *Division of Clinical Neuroscience, Center for Forensic Mental Health, Chiba University, 1-8-1 Inohana, Chiba 260-8670, Japan*

Received 21 October 2011; received in revised form 16 May 2012; accepted 2 June 2012
Available online 27 June 2012

KEYWORDS
Serine racemase;
D-Serine;
NMDA receptor;
Clonic–tonic seizure;
c-Fos;
Glutamate

Summary The *N*-methyl-D-aspartate (NMDA)-type glutamate receptor plays a key role in excitatory synaptic transmission. The overactivation of the NMDA receptor has been implicated in the development of epileptic seizures. D-Serine is a coagonist of the NMDA receptor and its biosynthesis is catalyzed by serine racemase (SR). Here, we examined the effect of D-serine deficiency on the seizures induced by a single injection of pentylenetetrazole (PTZ) using SR knockout (KO) mice. We found that, compared with wild-type (WT) mice, SR-KO mice showed the attenuation of seizure expression in terms of a significantly shortened duration of generalized seizures and resistance to generalized clonic–tonic seizures. Consistently, immunohistochemical analysis of c-Fos demonstrated that the numbers of cells expressing c-Fos induced by high-dose PTZ in the cerebral cortex, hippocampal CA1, hippocampal CA3, and the basolateral nucleus of the amygdala in WT mice were significantly higher than those in SR-KO mice. Moreover, PTZ induced an increase in extracellular glutamate level in the dentate gyrus of WT mice at two different time phases. However, such a PTZ-induced increase in glutamate level was completely inhibited in SR-KO mice. The present findings suggest that SR may be a target for the development of new therapeutic strategies for epileptic seizures.

Introduction

Epilepsy is a serious brain disorder, characterized by spontaneous and recurrent seizures. Seizures may result from intense neuronal discharges that are generated by the synchronized activity of a large number of neurons in

* Corresponding author. Tel.: +81 76 434 7230; fax: +81 76 434 5015.
E-mail address: hmori@med.u-toyama.ac.jp (H. Mori).
[1] Co-first authors.

0920-1211/$ – see front matter © 2012 Elsevier B.V. All rights reserved.
http://dx.doi.org/10.1016/j.eplepsyres.2012.06.001

different brain regions, which is basically caused by an imbalance between excitatory and inhibitory neurotransmissions (Cloix and Hevor, 2009; McCormick and Contreras, 2001). Glutamate is an amino acid neurotransmitter mediating excitatory synaptic transmission in the central nervous system (Sahai, 1990) and its excessive release has been implicated in the generation and maintenance of epileptic seizures (During and Spencer, 1993; Meldrum, 1994).

The *N*-methyl-D-aspartate (NMDA)-type glutamate receptor plays key roles in excitatory synaptic transmission, plasticity, and learning and memory (Bliss and Collingridge, 1993). The overactivation of the NMDA receptor has been demonstrated to be the mechanistic basis of numerous neurological disorders characterized by hyperexcitability or sensitization of neurons, including seizure disorders (Herron et al., 1986). Many in vitro and in vivo studies have focused on the pharmacological inhibition of the NMDA receptor as a therapeutic strategy for epilepsy, and a number of antagonists of the NMDA receptor were proven to have a potent anticonvulsant effect in a wide range of animal epileptic models (Brandt et al., 2003; Clifford et al., 1990; Croucher et al., 1982). However, their severe adverse effects have limited their clinical applications (Kohl and Dannhardt, 2001).

D-Serine, a D-amino acid abundant in the mammalian brain, is an endogenous ligand of the glycine site of the NMDA receptor (Hashimoto et al., 1992). The activation of the NMDA receptor requires, besides the binding of glutamate to the GluN2 (NR2) subunit, the binding of glycine or D-serine to the glycine site on the GluN1 (NR1) subunit (Dingledine et al., 1999). D-Serine is efficacious in potentiating the activity of the NMDA receptor (Fadda et al., 1988; Matsui et al., 1995) and its deletion was demonstrated to greatly decrease NMDA receptor activity (Mothet et al., 2000).

D-Serine is synthesized by serine racemase (SR), an enzyme that directly converts L-serine into D-serine (Wolosker et al., 1999). To investigate the role of D-serine in brain function, we have generated SR gene knockout (KO) mice with a 90% decrease in D-serine level and demonstrated that NMDA-receptor-mediated neurodegeneration can be attenuated in SR-KO mice (Miya et al., 2008; Inoue et al., 2008).

In the present study, we hypothesized that the D-serine deficiency in SR-KO mice has an anticonvulsant effect; thus, we compared the severity of seizures induced by a single injection of pentylenetetrazole (PTZ), a well-known antagonist of the gamma-aminobutyric acid ($GABA_A$) receptor (Fisher, 1989), between wild-type (WT) and SR-KO mice. Furthermore, as responses to PTZ-induced seizures, the changes in the level of c-Fos expression, an indicator of neuronal activation (Dragunow and Robertson, 1988; Sagar et al., 1988), and in extracellular glutamate level in the dentate gyrus (DG) of the hippocampus were also examined in these two genotypes.

Methods

Animals

Animal care and experimental protocols were carried out basically in accordance with the "Guidelines for the Care and Use of Laboratory Animals, DHEW, publication no. (NIH) 80–23, revised 1996" and approved by the Experimental Animal Committee of the University of Toyama (Authorization No. 2010-MED-61). The SR-KO mice with 100% C57BL/6 genetic background were generated as previously reported (Miya et al., 2008). The loss of SR mRNA and its protein in SR-KO mice has been confirmed by Northern blot, Western blot, and immunohistochemical analyses as previously reported (Miya et al., 2008; Inoue et al., 2008). The WT and SR-KO mice at the age of 9–13 weeks were used for analyses in a genotype-blind manner.

Seizure observation procedures

PTZ (Sigma–Aldrich Corp., St. Louis, MO, USA) was dissolved in sterile saline and administered intraperitoneally (i.p.) at doses of 35, 50, and 65 mg/kg body weight. Immediately after the single injection of PTZ, the mice were placed in clear polyvinyl chloride boxes and their behaviors were recorded on videotapes for 30 min.

On the basis of a previous report (Ferraro et al., 1999), PTZ-induced seizures were classified into four stages. Stage 1 was defined as hypoactivity, characterized by the animal being in the resting position with the abdomen fully touching the bottom of the cage. Stage 2 was defined as partial clonus, including that of the face, head, or forelimbs. Stage 3 was defined as generalized clonus, consisting of rearing, falling, and clonus of all four limbs and the tail. Stage 4 was defined as clonic–tonic (maximal) seizure, involving tonic hindlimb extension or death. Both stages 3 and 4 were considered as generalized seizures. In addition, the latency to the onset of the first seizure and the duration of generalized seizures were recorded.

Immunohistochemical analysis

Two hours after PTZ injection, the mice were sacrificed by cervical dislocation and decapitation. The brains were removed immediately and fixed overnight at 4 °C in 0.1 M phosphate buffer (PB, pH 7.4) containing 4% (w/v) paraformaldehyde. After cryoprotection with 30% (w/v) sucrose in PB, the brains were cut into 25-μm-thick serial coronal sections using a freezing microtome. For each animal, every eighth section (bregma from −1.58 mm to −2.46 mm, 5 sections/animal) was selected on the basis of the mouse brain in stereotaxic coordinates (Paxinos and Franklin, 2001) and was prepared for immunohistochemical analysis as follows.

Free-floating brain sections were rinsed with phosphate-buffered saline (PBS, pH 7.4) and were blocked with Protein Block Serum-Free (DakoCytomation, Carpinteria, CA) for 10 min at room temperature. The brain sections were then incubated with a rabbit anti-c-Fos polyclonal antibody (Santa Cruz Biotechnology, Santa Cruz, CA, 1:500) diluted in PBS containing 1% bovine serum albumin (BSA) overnight at 4 °C. After washing in PBS, the sections were incubated with donkey anti-rabbit IgG conjugated with Alexa Fluor 488 (Invitrogen, Carlsbad, CA, 1:500) diluted in PBS containing 1% BSA for 1 h at room temperature. The sections were washed in PBS, mounted on slides, counterstained with 4′,6-diamidino-2-phenylindole (DAPI, Vector, Burlingame, CA), and coverslipped.